



Evaluation of global fire simulations in CMIP6 Earth system models

Fang Li¹, Xiang Song¹, Sandy P. Harrison², Jennifer R. Marlon³, Zhongda Lin⁴, L. Ruby Leung⁵, Jörg Schwinger⁶, Virginie Maréchal⁷, Shiyu Wang⁸, Daniel S. Ward⁹, Xiao Dong¹, Hanna Lee¹⁰, Lars Nieradzik¹¹, Sam S. Rabin¹², and Roland Séférian⁷

¹International Center for Climate and Environment Sciences, Institute of Atmospheric Physics, Chinese Academy of Sciences, Beijing, 100029, China

²Department of Geography and Environmental Science, University of Reading, Reading, RG6 6AB, UK

³School of the Environment, Yale University, New Haven, CT 06511, USA

⁴State Key Laboratory of Numerical Modeling for Atmospheric Sciences and Geophysical Fluid Dynamics, Institute of Atmospheric Physics, Chinese Academy of Sciences, Beijing, 100029, China

⁵Atmospheric, Climate, and Earth Sciences Division, Pacific Northwest National Laboratory, Richland, WA 99354, USA

⁶NORCE Norwegian Research Centre and Bjerknes Centre for Climate Research, Bergen, 5838, Norway

⁷Centre National de Recherches Météorologiques, Université de Toulouse, Météo-France, CNRS, Toulouse, 31000, France

⁸Swedish Meteorological and Hydrological Institute (SMHI), Norrköping, 60176, Sweden

⁹Karen Clark & Company, Boston, MA 02116, USA

¹⁰Department of Biology, Norwegian University of Science and Technology, Trondheim, 7419, Norway

¹¹Department of Physical Geography and Ecosystem Science, Lund University, Lund, 22362, Sweden

¹²Climate and Global Dynamics Laboratory, National Center for Atmospheric Research, Boulder, CO 80305, USA

Correspondence: Fang Li (lifang@mail.iap.ac.cn)

Received: 1 May 2024 – Discussion started: 15 May 2024

Revised: 2 October 2024 – Accepted: 18 October 2024 – Published: 11 December 2024

Abstract. Fire is the primary form of terrestrial ecosystem disturbance on a global scale and an important Earth system process. Most Earth system models (ESMs) have incorporated fire modeling, with 19 of them submitting model outputs of fire-related variables to the Coupled Model Inter-comparison Project Phase 6 (CMIP6). This study provides the first comprehensive evaluation of CMIP6 historical fire simulations by comparing them with multiple satellite-based products and charcoal-based historical reconstructions. Our results show that most CMIP6 models simulate the present-day global burned area and fire carbon emissions within the range of satellite-based products. They also capture the major features of observed spatial patterns and seasonal cycles, the relationship of fires with precipitation and population density, and the influence of the El Niño–Southern Oscillation (ENSO) on the interannual variability of tropical fires. Regional fire carbon emissions simulated by the CMIP6 models from 1850 to 2010 generally align with the charcoal-based reconstructions, although there are regional mismatches, such as in southern South America and eastern

temperate North America prior to the 1910s and in temperate North America, eastern boreal North America, Europe, and boreal Asia since the 1980s. The CMIP6 simulations have addressed three critical issues identified in CMIP5: (1) the simulated global burned area being less than half of that of the observations, (2) the failure to reproduce the high burned area fraction observed in Africa, and (3) the weak fire seasonal variability. Furthermore, the CMIP6 models exhibit improved accuracy in capturing the observed relationship between fires and both climatic and socioeconomic drivers and better align with the historical long-term trends indicated by charcoal-based reconstructions in most regions worldwide. However, the CMIP6 models still fail to reproduce the decline in global burned area and fire carbon emissions observed over the past 2 decades, mainly attributed to an underestimation of anthropogenic fire suppression, and the spring peak in fires in the Northern Hemisphere mid-latitudes, mainly due to an underestimation of crop fires. In addition, the model underestimates the fire sensitivity to wet–dry conditions, indicating the need to improve fuel wet-

ness estimation. Based on these findings, we present specific guidance for fire scheme development and suggest a post-processing methodology for using CMIP6 multi-model outputs to generate reliable fire projection products.

1 Introduction

Fire is the primary form of terrestrial ecosystem disturbance on a global scale and a critical Earth system process (Randerson et al., 2006; Bowman et al., 2009). Fire has occurred since the emergence of terrestrial plants over 400 million years ago (Scott and Glasspool, 2006; Bowman et al., 2009) and presently burns more than 400 Mha of vegetated land and emits 2–3 Pg carbon globally each year (van der Werf et al., 2017; Giglio et al., 2018; Chuvieco et al., 2018; Chen et al., 2023). Fire is regulated by climate and weather, vegetation characteristics, and human activities and at the same time influences them in multiple ways, resulting in intricate feedback loops (Bond-Lamberty et al., 2007; Jiang et al., 2016; Li and Lawrence, 2017; Li et al., 2017, 2019; Lasslop et al., 2020; Kim et al., 2020; Wu et al., 2022; Lou et al., 2023). Despite a reduction in the global burned area over the past 2 decades, emissions from forest fires and the occurrence of extreme fires have increased (Andela et al., 2017; Zheng et al., 2021). Moreover, global fires are projected to rise in most regions of the world, particularly if climate mitigation efforts are weak (Li et al., 2021; Yu et al., 2022; UNEP, 2022).

Earth system models (ESMs) simulate the processes and interactions within and across the atmosphere, the land, the ocean, sea ice, and the biosphere, which are crucial for analyzing historical climate and environmental changes and for projecting the Earth's future (Scholze et al., 2013; Danabasoglu et al., 2020; Song et al., 2021). ESMs became the predominant coupled model type in the Coupled Model Intercomparison Project Phase 6 (CMIP6; Eyring et al., 2016), which is the latest iteration of CMIP to release model outputs for general use and supports the Intergovernmental Panel on Climate Change Sixth Assessment Report (IPCC AR6; IPCC, 2021). Given the critical role of fire in the Earth system, most ESMs already include fire modeling.

Kloster and Lasslop (2017) assessed fire simulations in CMIP5 based on nine models that had submitted historical fire simulations. They found these models severely underestimated the global burned area by more than 50 % compared to observations, although the simulated global fire carbon emissions were within the range of observations. They also showed that all CMIP5 models failed to reproduce the spatial patterns of the burned area, mainly because they underestimated the high values in Africa, and only MPI-ESM performed better than a random model in simulating the observed seasonal phase of burned area. The most used fire scheme in CMIP5 models was GlobFIRM (Thonicke et al., 2001), which has several limitations that explain the short-

comings in CMIP5 coupled model fire simulations. GlobFIRM calculates annual burned area fraction as a nonlinear function of fire season length, which is determined by summing fire occurrence probability over a year. This approach leads to underestimation in grid cells where multiple fires occur in a single time step because the probability cannot exceed 1. Additionally, the lack of observational data for fire occurrence probability makes it impossible to calibrate fire occurrence parameters. GlobFIRM's annual burned area simulation cannot capture fire seasonality. While some models modified GlobFIRM to operate at sub-daily to monthly time steps by using weighted differences in running annual mean burned areas, the Kloster and Lasslop (2017) evaluation showed that this modification did not result in skillful simulations of burned area seasonality.

Many more models have conducted fire-enabled historical simulations for CMIP6, in which the most used fire scheme has evolved from the GlobFIRM scheme in CMIP5 to the Li scheme (Li et al., 2012, 2013; Li and Lawrence, 2017). However, it remains unknown how well CMIP6 ESMs perform in fire simulations. This study provides the first comprehensive evaluation of CMIP6 fire simulations, including the global total, spatial pattern, seasonality, recent and historical trends, and interannual variability of burned area and fire carbon emissions. To disentangle biases and inter-model differences arising from fire parameterization schemes and climate simulations, we also evaluate the modeled relationship between fires and two key driving variables: precipitation in the tropics and subtropics (35° S to 35° N) and population density globally. This evaluation can deepen our understanding of past, present, and future changes in fires, as well as the closely related carbon cycle, within CMIP6 simulations. Based on the results, we also suggest strategies for fire scheme development and for the post-processing methodology of CMIP6 multi-model ensemble simulations to generate more reliable projections of future fire changes.

2 Data and methods

2.1 Fire simulations

We downloaded CMIP6 historical fire simulations that cover the period of 1850–2014 from <http://esgf-node.llnl.gov/search/cmip6/> (last access: March 2023) (Eyring et al., 2016). A total of 19 ESMs submitted fire simulations, of which 9 models submitted burned area, and 18 models submitted fire carbon emissions (Table 1). All the simulations were driven by the same forcing data, e.g., prescribed greenhouse gas concentration (Meinshausen et al., 2017), anthropogenic and biomass burning emissions (Feng et al., 2020), and land use and land cover change (Hurtt et al., 2020).

The fire schemes employed in all 19 ESMs are process based, simulating the processes of both fire occurrence and fire spread. Of the nine models providing burned

Table 1. Summary description of CMIP6 ESMs used in the study.

ESMs	Institute	BA	Fire C	Land model	Fire scheme	Human ign/sup	Crop fires
AWI-ESM-1-1-LR	AWI (Germany)		✓	JSBACH3.2	SPITFIRE ^d (modified)	✓/✓	0
CESM2	NCAR (USA)	✓	✓	CLM5	Li ^a	✓/✓	✓
CESM2-WACCM	NCAR (USA)	✓	✓	CLM5	Li ^a	✓/✓	✓
CMCC-CM2-SR5	CMCC (Italy)	✓	✓	CLM4.5	Li ^b	✓/✓	✓
CMCC-ESM2	CMCC (Italy)	✓	✓	CLM4.5	Li ^b	✓/✓	✓
CNRM-ESM2-1	CNRM-CERFACS (France)	✓	✓	ISBA-CTRIIP	GlobFIRM ^e (modified)	/✓	0
E3SM-1-1	DOE (USA)		✓	ELM	Li ^b	✓/✓	✓
E3SM-1-1-ECA	DOE (USA)		✓	ELM	Li ^b	✓/✓	✓
EC-Earth3-CC	EC-Earth-Cons. (Europe)	✓	✓	LPJ-GUESS	GlobFIRM		
EC-Earth3-Veg	EC-Earth-Cons. (Europe)	✓	✓	LPJ-GUESS	GlobFIRM		
EC-Earth3-Veg-LR	EC-Earth-Cons. (Europe)		✓	LPJ-GUESS	GlobFIRM		
GFDL-ESM4	NOAA-GFDL (USA)		✓	LM4.1	FINAL ^f Li ^c	✓/✓	✓
MPI-ESM1-2-HAM	HAMMOZ-Cons. (Europe)		✓	JSBACH3.2	SPITFIRE ^d (modified)	✓/✓	0
MPI-ESM1-2-LR	MPI (Germany)		✓	JSBACH3.2	SPITFIRE ^d (modified)	✓/✓	0
MRI-ESM2-0	MRI (Japan)		✓	HAL1	GlobFIRM		
NorCPM1	NCC (Norway)		✓	CLM4	GlobFIRM		
NorESM2-LM	NCC (Norway)	✓	✓	CLM5	Li ^b	✓/✓	✓
NorESM2-MM	NCC (Norway)	✓	✓	CLM5	Li ^b	✓/✓	✓
TaiESM1-0	AS-RCEC (Taiwan)		✓	CLM4	GlobFIRM ^g	✓/✓	

^a Li et al. (2012, 2013) and Li and Lawrence (2017); ^b Li et al. (2012, 2013); ^c Li et al. (2012); ^d SPITFIRE (Thonicke et al., 2010) with modifications from Lasslop et al. (2014); ^e GlobFIRM (Thonicke et al., 2001) but adapted to a daily time step, tuning parameters, and assuming no fire in the grid cell where the cropland fraction is over 20%; ^f FINAL (Li et al., 2012) but tuning parameters and using prescribed cropland and pasture fires based on GFED3 (Rabin et al., 2018), as well as introducing the landscape fragmentation effect on fire spread, multiday burning, and the SPITFIRE canopy fire scheme (Ward et al., 2018); ^g GlobFIRM (Thonicke et al., 2001) but adapted to a sub-hourly time step (Kloster et al., 2010).

References for ESMs: AWI-ESM-1-1-LR (Contzen et al., 2022), CESM2 family (Danabasoglu et al., 2020), CMCC-CM2-SR5 (Cherchi et al., 2019), CMCC-ESM (Lovato et al., 2022), CNRM-ESM2-1 (Séférian et al., 2019), E3SM-1-1 and E3SM-1-1-ECA (Burrows et al., 2020), EC-Earth3 family (Döscher et al., 2022), GFDL-ESM4 (Dunne et al., 2020), MPI-ESM1-2-HAM (Neubauer et al., 2019), MPI-ESM1-2-LR (Mauritsen et al., 2019), MRI-ESM2-0 (Yukimoto et al., 2019), NorCPM1 (Bethke et al., 2021), NorESM2 family (Seland et al., 2020), and TaiESM1-0 (Lee et al., 2020).

Human ign/sup: human ignitions or suppression.

area data, six used the Li scheme (Li et al., 2012, 2013; Li and Lawrence, 2017), while the remaining three utilized the GlobFIRM scheme (Thonicke et al., 2001). Among the 18 models that provided fire carbon emissions data, 8 adopted the Li scheme, 7 employed the GlobFIRM scheme, and 3 used the modified SPITFIRE scheme (Thonicke et al., 2010) by Lasslop et al. (2014). The SPITFIRE scheme is the most complex since it uses the Rothermel model to calculate the fire spread rate in the downwind direction, considers the impact of the fuel structure, and distinguishes surface and canopy fires. On the other hand, Li's scheme employs a simple empirical function in which the fire spread rate in the downwind direction is determined by fuel wetness and wind speed, and GlobFIRM does not calculate the fire spread rate at all. The fire schemes differ in their fundamental equations for calculating the burned area. The Li fire scheme and SPITFIRE calculate the time step of the burned area in a grid cell as a product of the number of fires and the average spread area per fire. For GlobFIRM, the annual burned area fraction is a nonlinear function of fire season length, in which the fire

season length is calculated by summing fire occurrence probability throughout the year. CNRM-ESM2-1 modifies the annual calculation of GlobFIRM to a daily time step using the methodology of Krinner et al. (2005) for simulations of fire seasonality (Delire et al., 2020).

The fire schemes also vary in how they model anthropogenic influence on fires (Table 1). GlobFIRM does not account for direct human effects on fires, but its variant (used in CNRM-ESM2-1) considers human suppression by assuming no fire occurrence when croplands cover more than 20% of the grid cell. The Li scheme models crop fires, fires caused by anthropogenic deforestation in tropical closed forests, and human ignition and suppression of both fire occurrence and spread in regions outside of tropical closed forests and croplands. However, in the CESM2, CESM2-WACCM, NorESM2-LM, and NorESM2-MM simulations for CMIP6, the crop module was active and assumed no fires occurred in managed croplands. The variant of SPITFIRE used in MPI-ESM1-2-HAM, MPI-ESM1-2-LR, and MPI-ESM2-0 also considers the effect of human

ignition and suppression on fire occurrence and sets burned area to zero in croplands. In addition, all the ESMs treat fires in pasturelands as natural grassland fires, except for GFDL-ESM4.1, which uses prescribed pasture fires derived from the multi-year average burned area of the Global Fire Emissions Database version 3 with small fires (GFED3s) (Rabin et al., 2018). The MPI-ESM family (using a variant of SPITFIRE) sets high fuel bulk density for the pasture plant functional types (PFTs), which indirectly distinguishes these from natural grassland fires due to differences in fuel availability.

The fire schemes calculate fire carbon emissions by multiplying the burned area, fuel load, and combustion completeness. The combustion completeness is a proportion (0%–100%) of live plant tissues and ground litter consumed by fires. It depends on PFT and plant tissue type in both the GlobFIRM scheme and the Li scheme and on fuel type and wetness in SPITFIRE.

For comparison, we downloaded CMIP5 historical fire simulations from <http://esgf-node.llnl.gov/search/cmip5/> (last access: March 2023). The CMIP5 historical simulations cover the period from 1850 to 2005 (Taylor et al., 2012) and thus end 9 years earlier than CMIP6 historical simulations. Seven models submitted burned area simulations in CMIP5 (CCSM4, CESM1-BGC, CESM1-CAM5, CESM1-FASTCHEM, CESM1-WACCM, MPI-ESM-LR, and MPI-ESM-MR), and 12 models submitted fire carbon emissions simulations (BNU-ESM, CCSM4, CESM1-BGC, CESM1-FASTCHEM, CESM1-WACCM, CMCC-CESM, GFDL-ESM2G, GFDL-ESM2M, IPSL-CM5-LR, IPSL-CM5-MR, MPI-ESM-LR, and MPI-ESM-MR). The majority of the CMIP5 models (5 out of 7 and 8 out of 12) used the GlobFIRM fire scheme (Thonicke et al., 2001) but adapted the scheme's annual time step to a sub-daily to monthly time step using a similar method to CNRM-ESM2-1 in CMIP6 (Krinner et al., 2005; Kloster et al., 2010; Kloster and Lasslop, 2017).

2.2 Fire benchmarks

There are differences between satellite-based fire products (Li et al., 2019; Hantson et al., 2020). To account for the uncertainty in observations, we employed multiple products as benchmarks.

For burned area, we used the Global Fire Emissions Database version 5 (GFED5; Chen et al., 2023), the European Space Agency Fire Climate Change Initiative version 5.1 (FireCCI51; Chuvieco et al., 2018), and the Collection 6 Moderate Resolution Imaging Spectroradiometer (MODIS C6; Giglio et al., 2018), all of which provide monthly data at 0.25° spatial resolution. We used the period of 2001–2014 to compare with the CMIP6 historical simulations. Burned area since 2001 in GFED5 is based on the MODIS global burned area product MCD64A1, with omission and commission errors corrected by dynamic adjustment factors estimated using the Landsat or Sentinel-

2 burned area (Chen et al., 2023). The FireCCI51 burned area is derived using the MODIS C6 250 m daily surface reflectance, MCD14ML 1 km daily active fire products, and a two-phase approach for seed detection and regional growth (Chuvieco et al., 2018). The MODIS C6 burned area is generated from the MODIS C6 Terra and Aqua 500 m daily surface reflectance products, MOD14A1 and MYD14A1 1 km daily level-3 active fire products, and the MCD12Q1 500 m annual land cover product (Giglio et al., 2018).

For present-day fire carbon emissions, we used GFED4s (van der Werf et al., 2017; GFED5 fire emissions have not been released), the Global Fire Assimilation System version 1.2 (GFAS1.2; Kaiser et al., 2012), and the Fire Energetics and Emissions Research version 1.0-G1.2 (FEER-G1.2; Ichoku and Ellison, 2014) as benchmarks. The GFED4s fire emissions from 1997 at 0.25° are constructed using the CASA biogeochemical model with GFED4s burned area and observed meteorology and vegetation as inputs (van der Werf et al., 2017). The 0.1° daily GFAS1.2 from 2003 to the present is based on observations of fire radiative power (FRP) from MODIS and the biome-specific conversion factors derived based on GFED3.1 dry matter burned. The 0.5° daily FEER-G1.2 fire emissions from 2003 are derived from MODIS FRP and constrained with the MODIS aerosol optical depth (AOD) product MOD04_L2 (Ichoku and Ellison, 2014). The three fire carbon emissions products represent the range of satellite-derived inventories well (Li et al., 2019; Wiedinmyer et al., 2023). We used the 2003–2014 period of these satellite products as it overlaps with the time frame of the CMIP6 historical simulations.

To evaluate long-term trends in fires starting from 1850, we used 992 charcoal records from the Reading Paleofire Database (RPD; Harrison et al., 2022). Sedimentary charcoal records reflect changes in biomass burning, which are primarily influenced by burned area (Haas et al., 2022) but are also affected by combustion completeness. In the CMIP6 simulations, biomass burning is represented by the variable of fire carbon emissions, and model-submitted fire carbon emissions are much more than submitted burned area. Consequently, this study examined the similarity in trends between these records and simulated fire carbon emissions. The largest number of records in the RPD is from North America and Europe, but there are enough records for other regions to construct trustworthy regional composites, except for Northern Hemisphere Africa (NHAF), Southern Hemisphere Africa (SHAF), and the Middle East (MIDE) (Fig. S1 in the Supplement).

2.3 Simulations and observations of fire drivers

We downloaded the CMIP6 model outputs of precipitation and sea surface temperature (SST) from <http://esgf-node.llnl.gov/search/cmip6/> (last access: March 2023) and CMIP5 precipitation simulations from <http://esgf-node.llnl.gov/search/cmip5/> (last access: March 2023).

Observed 0.5° monthly precipitation observations were obtained from the Climatic Research Unit Time-series version 4.04 (CRU TS v.4.04) (Harris et al., 2020). The 1870–2023 1° monthly SST observations were from the Hadley Centre Sea Ice and Sea Surface Temperature (HadISST) data set (Rayner et al., 2003). Annual population density data from 1850 to 2014 at 0.5° spatial resolution were taken from HYDEv3.2 (Klein Goldwijk et al., 2017), which were also used to drive the CMIP6 models.

2.4 Data processing

For CMIP6 fire simulations, we corrected unit errors and then uniformly adopted $\% \text{ mon}^{-1}$ for the burned area fraction and $\text{kgCm}^{-2}\text{s}^{-1}$ for fire carbon emissions. The data were then regridded to a 1° spatial resolution using bilinear interpolation for coarser-resolution simulations and area-weighted averaging for finer-resolution simulations and satellite-based products.

For RPD charcoal records, we constructed composite time series for different regions (Fig. S1) after rescaling the individual records using a minimax transformation, homogenizing the variance using the Box–Cox transformation, and rescaling the transformed values to z scores (Power et al., 2010). The composite curve for each region was constructed with decadal resolution and a base period from 1750 to 2010. The loess regression with a half-window width of 10 years was used to yield estimates for each decade. Uncertainties (95 %) were calculated by bootstrap resampling of the records 1000 times.

For the regional analysis, we divided the global land into 16 regions (Fig. 1). This was done by combining the 14 GFED regions with the 12 RPD regions.

The Niño3.4 index, a widely recognized indicator of the El Niño–Southern Oscillation (ENSO), is defined as the SST anomaly averaged over the central-eastern equatorial Pacific (5°S – 5°N , 120° – 170°W). Based on this definition, we calculated the simulated and observed Niño3.4 index.

2.5 Evaluation methods

Our evaluations focus on the total amount, spatial distribution, seasonal cycle, long-term trend, and interannual variability of burned area and fire carbon emissions, as well as the relationship between fires and climatic or socioeconomic factors.

The global and regional totals or averages of a variable were calculated as the area-weighted sum or average across global land areas and specific regions, respectively. The Pearson correlation coefficient between observations and simulations was used to evaluate the skill of spatial and temporal variability patterns, and Student's t test was used to assess their significance. To test the significance of the spatial correlation, the effective degrees of freedom (EDOFs) were estimated via the widely used method of Bayley and Hammer-

sley (1946) and Clifford et al. (1989), in which autocorrelation in observed and simulated spatial patterns reduces the EDOFs, thereby raising the thresholds for statistical significance.

We estimated the long-term trend using the ordinary least squares (OLS) method and evaluated its significance using the Mann–Kendall test.

The coefficient of variation (CV; standard deviation divided by the average) was used to quantify the magnitude of interannual variability and seasonality. Given that ENSO is the dominant driver of the interannual variability of pan-tropical fires (Chen et al., 2017), we evaluated simulations of fire interannual variability using the correlation between detrended tropical fires and the detrended Niño3.4 index.

When evaluating the relationship between fire and its drivers, we examined how the annual burned area fraction in the tropics and subtropics (35°S to 35°N) varied with annual precipitation, following Prentice et al. (2011) and Kloster and Lasslop (2017), and how the global annual burned area fraction changed with population density as in Li et al. (2018).

3 Results

3.1 Global totals

The present-day global burned area estimated by six out of nine CMIP6 models and the multi-model ensemble (MME) fall within the range of satellite-based products (430 – 802 Mha yr^{-1}) (Fig. 2a). CMIP6 models perform much better than CMIP5 models (150 – 184 Mha yr^{-1} , below half the area shown by the benchmarks). The inter-model discrepancy of CMIP6 models is larger than that of the CMIP5 models, primarily due to the large difference in the three models that incorporate the GlobFIRM fire scheme and its variant (764 , 172 , and 176 Mha yr^{-1} for CNRM-ESM2-1, EC-Earth3-CC, and EC-Earth3-Veg, respectively). CNRM-ESM2-1 tuned the parameters of GlobFIRM based on fire occurrence measurements to obtain a more reasonable estimate of the global burned area (Delire et al., 2020).

The global totals of fire carbon emissions estimated by 11 out of 18 CMIP6 models fall within the range of benchmarks, as does the MME (Fig. 1b). The CMIP6 ensemble mean outperforms the CMIP5 ensemble mean, although inter-model differences are larger, mainly due to the anomalously low value of NorCPM1. Overall, EC-Earth3 models in CMIP6 and most CMIP5 models that use the GlobFIRM scheme reasonably simulate the global total of fire carbon emissions, even though the estimated global burned area is less than half that of the observed values. This is mainly because GlobFIRM uses higher combustion completeness factors for woody tissues (70 %–90 % for stem and coarse woody debris) than those used in Li (27 %–35 % for stem and 40 % for coarse woody debris), SPITFIRE (0 %–73 % for 100 h fuel type and 0 %–41 % for 1000 h fuel type) (Li

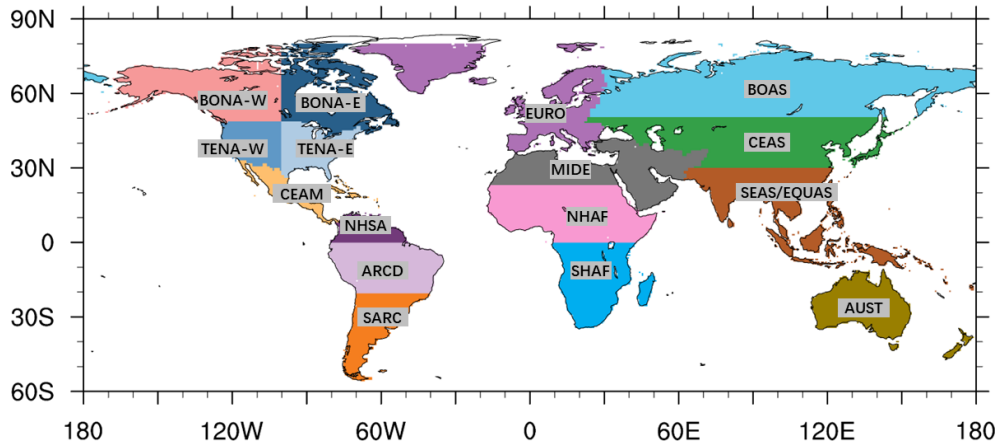


Figure 1. The definition of 16 regions used in this study, which combines the GFED regions and RPD regions. BONA-W – boreal North America-west, BONA-E – boreal North America-east, TENA-W – temperate North America-west, TENA-E – temperate North America-east, CEAM – Central America, NHSA – Northern Hemisphere South America, ARCD – arc of deforestation, SARC – south of the arc of deforestation, EURO – Europe, BOAS – boreal Asia, MIDE – Middle East, CEAS – central Asia, NHAF – Northern Hemisphere Africa, SHAF – Southern Hemisphere Africa, SEAS/EQUAS – Southeast Asia/equatorial Asia, AUST – Australia.

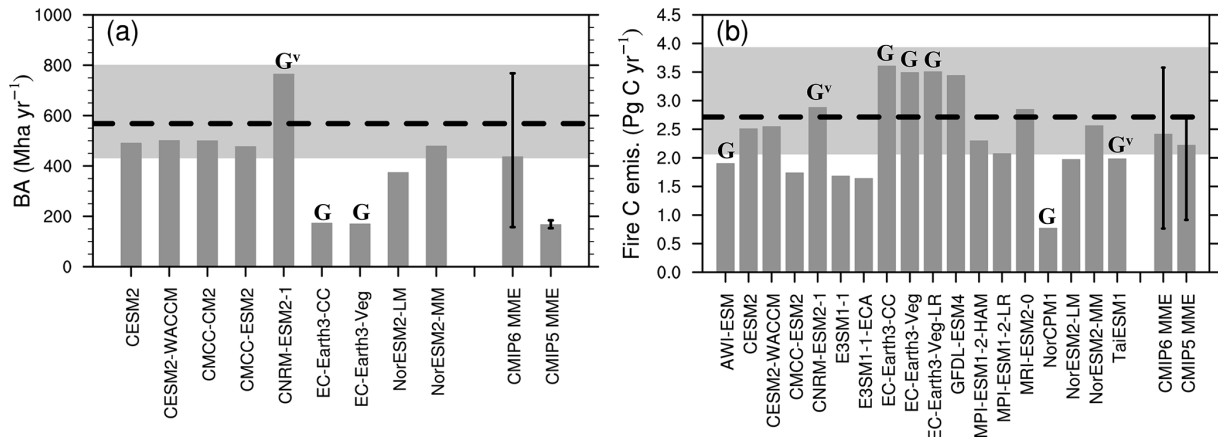


Figure 2. Present-day global totals of (a) burned area and (b) fire carbon emissions for benchmark averages (dashed lines) and model simulations (bars). The shaded areas show the range of the benchmarks, and error bars show the range of the models. The assessment is made for 2001–2014 for burned area and 2003–2014 for fire carbon emissions. The CMIP multi-model ensembles span 2001–2005 for burned area and 2003–2005 for fire carbon emissions. G and G^v denote models that use GlobFIRM or its variant. Other models used the Li fire scheme in (a) and Li or modified SPITFIRE in (b).

et al., 2019), and the satellite-based GFED family (20%–40% for stem and 40%–60% for coarse woody debris) (van der Werf et al., 2017). CNRM-ESM2-1 employs GlobFIRM but decreases the completeness factors to obtain a reasonable estimate of fire carbon emissions (Delire et al., 2020).

3.2 Spatial pattern

All the CMIP6 models capture key features of the observed spatial pattern of present-day burned area fraction, with global spatial correlations between simulations and observations that are statistically significant at the 0.05 level (Fig. 3). CMIP6 models outperform CMIP5 models in simulating spatial patterns, with correlation coefficients increasing from a

range of 0.15–0.34 in CMIP5 (Fig. S2 in the Supplement) to 0.28–0.70 in CMIP6. CMIP6 models incorporating the Li fire scheme have even higher correlations, ranging from 0.54 to 0.70. Most CMIP6 models successfully reproduce the observed high values in Africa, except for EC-Earth3-CC and EC-Earth3-Veg, which both use GlobFIRM (Fig. 3). However, CMIP6 models, except for EC-Earth3 family models, overestimate burned area in South American savannas (Fig. 3; Table S1 in the Supplement), possibly due to the underestimation of precipitation in this region during the fire seasons (Fig. S5 in the Supplement). Additionally, models using GlobFIRM overestimate the burned area in the western United States and tropical rainforests, whereas those using

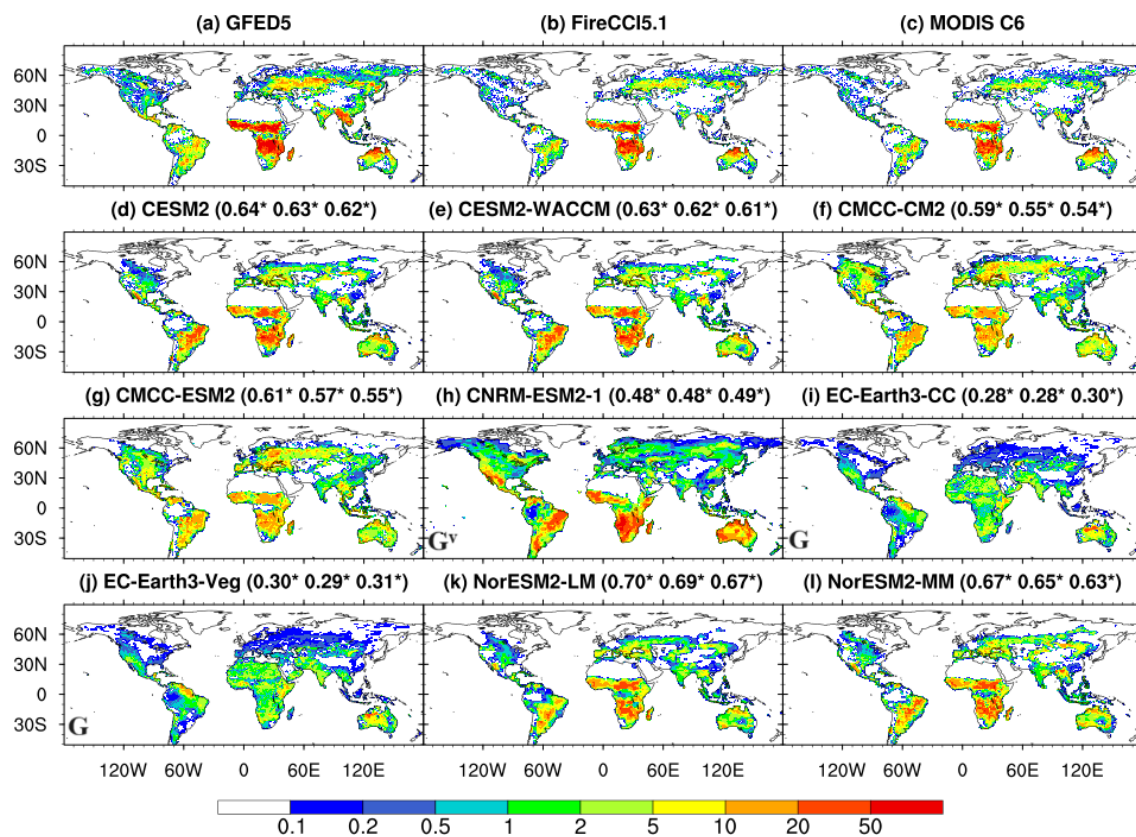


Figure 3. The 2001–2014 spatial distribution of the annual burned area fraction ($\% \text{ yr}^{-1}$) for (a–c) benchmarks and (d–l) CMIP6 models. The spatial correlations of simulations with three benchmarks are also given in parentheses. * – correlation significant at the 0.05 level based on Student’s t test with estimated effective degrees of freedom (EDOFs), which consider the impacts of autocorrelation in observed and simulated spatial patterns. G and G^V denote models using the GlobFIRM fire scheme and its variant, respectively, while the other models use the Li scheme.

the Li scheme typically underestimate it in boreal shrublands, possibly because the wet and cold bias during the fire season in the ESM climate simulations (Figs. S3c in the Supplement and 4c) leads to underestimations of fuel flammability.

The significant underestimation of burned area in EC-Earth3 models in CMIP6 for Africa (around 1/5 and 1/10 of observations for NH and SH Africa, respectively, as shown in Fig. 3 and Table S1) is primarily due to limitations of the GlobFIRM fire model they employ, as discussed in Sect. 4.2. However, climate simulation biases may also affect fire simulations to some extent. During fire seasons, EC-Earth3 exhibits a cool bias in NH Africa, similar to other CMIP6 models except CESM2 (Fig. S6l and n in the Supplement). This cool bias may decrease fuel flammability due to reduced water evaporation from fuel, leading to underestimation of burned area. In contrast, SH Africa shows a warm bias (Fig. S6k and m), which tends to cause an overestimation of burned area. During fire seasons, EC-Earth3 models show no significant precipitation biases and do not have larger precipitation biases than other ESMs in Africa (Fig. S5). Outside of fire seasons, EC-Earth3 models exhibit distinct precipitation

biases across Africa. In NH Africa, EC-Earth3 models show a dry bias (Fig. S5m and o); even though this dry bias is less pronounced than in CNRM-ESM2-1 (Fig. 5i), it may contribute to lower burned area estimates due to underestimated fuel load. In SH Africa, EC-Earth3 models display a wet bias, which potentially leads to higher burned area estimates due to overestimated fuel load. The CMIP6 models skillfully reproduce the observed spatial pattern of fire carbon emissions, except for MRI-ESM2, which utilizes GlobFIRM and incorrectly places the areas of high emissions north of 45° N (Fig. 4). The incorrect simulations of MRI-ESM2 (Fig. 4q) are likely due to a wet bias and particularly a large warm bias north of 45° N outside the fire season (Fig. S7 in the Supplement), which contributes to the accumulation of fuel for burning. Compared to CMIP5 models (Fig. S8 in the Supplement), CMIP6 models improve the simulations of spatial patterns, but the improvement is not as evident as that for the burned area fraction. The bias in the simulations of fire carbon emissions (Fig. 4, Table S2 in the Supplement) is similar to that for burned area fraction simulations. Models incorporating the complex SPITFIRE scheme do not outperform

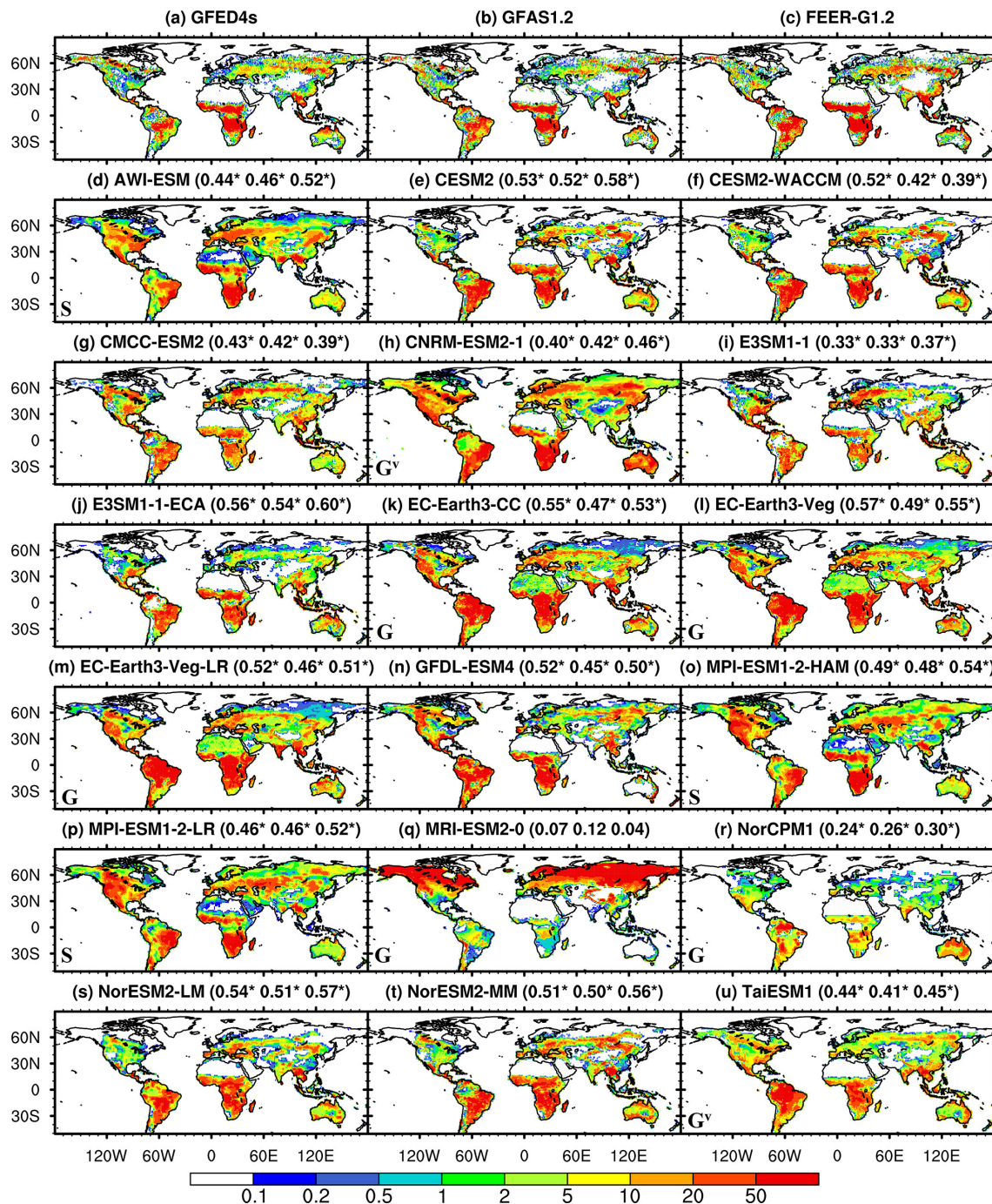


Figure 4. Same as Fig. 3 but for 2003–2014 fire carbon emissions ($\text{g C m}^{-2} \text{ yr}^{-1}$) for (a–c) benchmarks and (d–u) CMIP6 models. S indicates models using the SPITFIRE fire scheme.

simpler fire schemes, showing similar overestimations in the western United States and Arctic tundra to those using GlobFIRM (Fig. 4).

The CMIP6 MME exhibits an improved skill in simulating spatial patterns compared to CMIP5 MME, particularly for burned area fraction (Fig. 5). The global spatial correlation between simulations and observations for the CMIP6 MME

is 0.69, more than twice that for the CMIP5 MME (0.30). The most notable improvement in the burned area simulations is that CMIP6 models capture the observational high values in tropical savannas across Africa, South America, and Australia, as well as the moderate values observed in the boreal forests in Eurasia (Fig. 5a–c). CMIP6 MME outperforms CMIP5 MME for fire carbon emissions, mainly by reducing

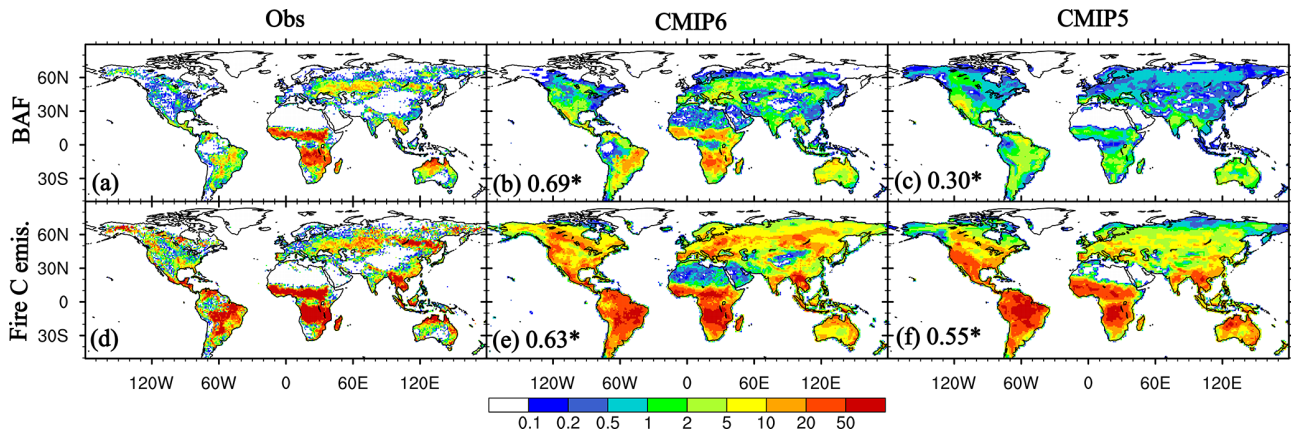


Figure 5. Spatial distribution of (a–c) annual burned area fraction (BAF; % yr⁻¹) averaged over 2001–2005 and (d–f) annual fire carbon emissions (gCm⁻²yr⁻¹) averaged over 2003–2005 for benchmark average (Obs), CMIP6 MME, and CMIP5 MME. The global spatial correlation between the simulation and observations is also given, with * representing a correlation significance at the 0.05 level. The benchmarks are GFED5, FireCCI5.1, and MODIS C6 for burned area and GFED4s, GFAS1.2, and FEER-G1.2 for fire carbon emissions.

the underestimation in Asian boreal forests and South Asia and the overestimation in western North America and South America (Fig. 5d–f). However, there are notable outliers in the simulations. The EC-Earth models, for instance, overestimate both burned area (Fig. 3i and j) and fire carbon emissions (Fig. 4k–m) in the Sahara region, likely due to an overestimation of fuel load (Song et al., 2021). As a result, the CMIP6 MMEs show some burned area and fire carbon emissions over the Sahara (Fig. 5b and e) due to these EC-Earth3 simulations. In contrast, MRI-ESM2 overestimates fire carbon emissions in regions north of 45° N (Fig. 4q).

3.3 Seasonal cycle

The CMIP6 models capture major features of the burned area seasonality: peak month occurs in the dry season in the tropics and in the warm season in the extra-tropics (Fig. 6). The CMIP6 models accurately capture the peak fire month in July–August in NH high latitudes (Fig. 6a and b) and January in SH mid-latitudes (Fig. 6i and j). The temporal correlation with observations ranges from 0.87 to 0.95 for the NH high latitudes and 0.57 to 0.70 for the SH mid-latitudes, all significant at the 0.05 level. On the contrary, most CMIP5 models fail to capture the seasonal phase of these regions (Fig. 6b and j).

In the NH tropics, the peak timing of CMIP6 models and the MME occurs in March, which is later than the observed peak in December–January (Fig. 6e and f). Despite this, they still outperform the CMIP5 models, which peak in March–May. In the SH tropics, both CMIP6 and CMIP5 models exhibit similar timing, peaking 1 or 2 months later than observed (Fig. 6g and h). The delays in fire peak timing for both CMIP5 and CMIP6 models are partly attributed to a simulation bias in precipitation, where the month with the

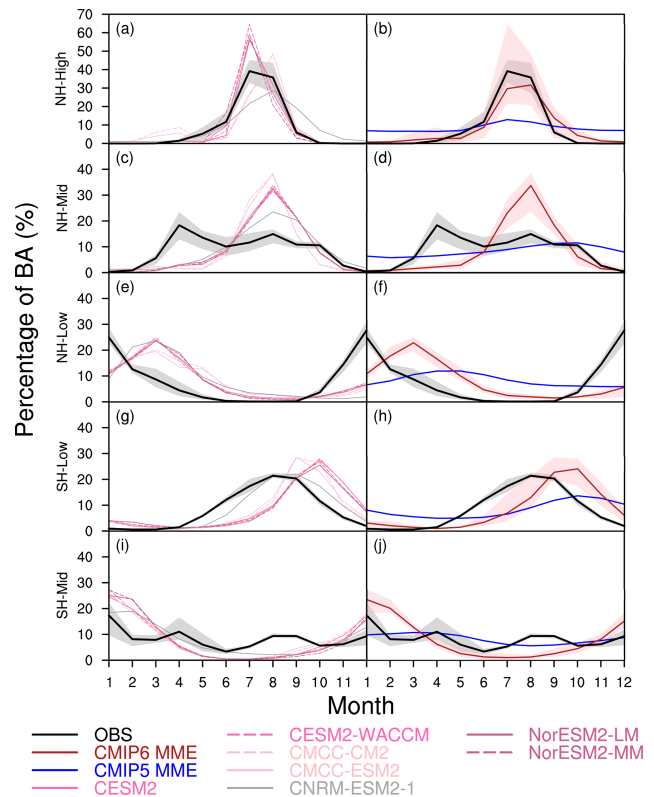


Figure 6. Seasonal cycle of burned area for observations and (a) CMIP6 models averaged over 2001–2014 or (b) CMIP6 and CMIP5 MMEs averaged over 2001–2005. Shaded areas show a range of benchmarks or models. EC-Earth3-CC and EC-Earth3-Veg do not model fire seasonal cycles and are thus excluded.

Table 2. Skill scores of seasonality simulations for CMIP6 and CMIP5 MMEs. The correlation coefficient and coefficient of variation (CV) are used to evaluate the phase and magnitude of seasonal variability, respectively. * – correlation significant at the 0.05 level.

	NH high	NH middle	NH low	SH low	SH middle
Correlation coefficient					
CMIP6-MME	0.98*	0.53*	0.22	0.58*	0.66*
CMIP5-MME	0.93*	0.20	−0.39	0.33	0.38
CV					
Obs	1.69	0.74	1.17	0.96	0.43
CMIP6-MME	1.73	1.28	0.88	1.02	0.99
CMIP5-MME	0.20	0.24	0.29	0.39	0.23

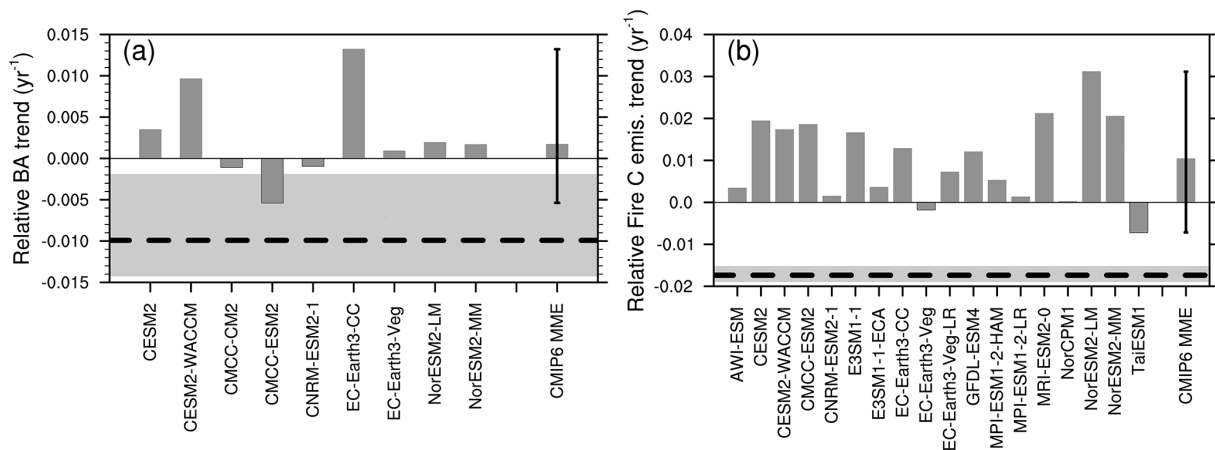


Figure 7. Same as Fig. 2 but for the relative trends in the present day (2001–2014 for the burned area and 2003–2014 for the fire carbon emissions).

minimum precipitation in the models occurs 1 or 2 months later than observed (Fig. S9 in the Supplement).

In the NH mid-latitudes, there are two observed fire peaks: one in spring, mainly caused by crop fires, and the other in summer, caused by fires occurring in natural vegetation areas (Fig. 6c). The CMIP6 models reproduce the summer peak with greater accuracy than the CMIP5 models, which peak 2 months later than the observations. However, neither the CMIP6 models nor the CMIP5 models capture the spring peak (Fig. 6c and d).

CMIP6 models reasonably simulate the magnitude of the seasonal variability of burned area and outperform CMIP5 models, except for the SH mid-latitudes (Fig. 6; Table 2). CMIP5 models severely underestimate the seasonal variation across all regions, simulating an abnormally flat seasonal cycle that represents only about 30 % of the observed variation (Table 2).

The performance of CMIP6 models in simulating the seasonal phase of fire carbon emissions is similar to that for burned area (Fig. S10 in the Supplement). Models using the Li and SPITFIRE schemes capture the peak in NH high latitudes (Fig. S8a and b) and the summer peak in NH mid-

latitudes (Fig. S10c and d). They exhibit a 1- to 2-month delay in the fire peak timing in NH and SH low latitudes (Fig. S10e–h). The peak in the SH mid-latitudes is captured accurately by models using the Li scheme but occurs 2 months later for SPITFIRE (Fig. S10i and j). In addition, different from the burned area simulations, both CMIP6 and CMIP5 models generally reproduce the observed magnitude of seasonal variability for fire carbon emissions (Fig. S10), although the CMIP5 models underestimate the seasonal variation in NH high latitudes (Fig. S10a and b) and SH mid-latitudes (Fig. S10i and j).

3.4 Trend

In recent decades, satellite-based products have revealed a significant decline in burned area and fire carbon emissions (dashed lines with shades in Fig. 7), but CMIP6 models do not capture this trend (bars in Fig. 7), similar to CMIP5 models (Kloster and Lasslop, 2017) and FireMIP dynamic global vegetation models (DGVMs) (Andela et al., 2017). Spatially, the observed decline in 2001–2014 burned area is most pronounced in tropical savannas in South America, NH Africa, and Australia, showing significant trends of -1.9 to -0.4 ,

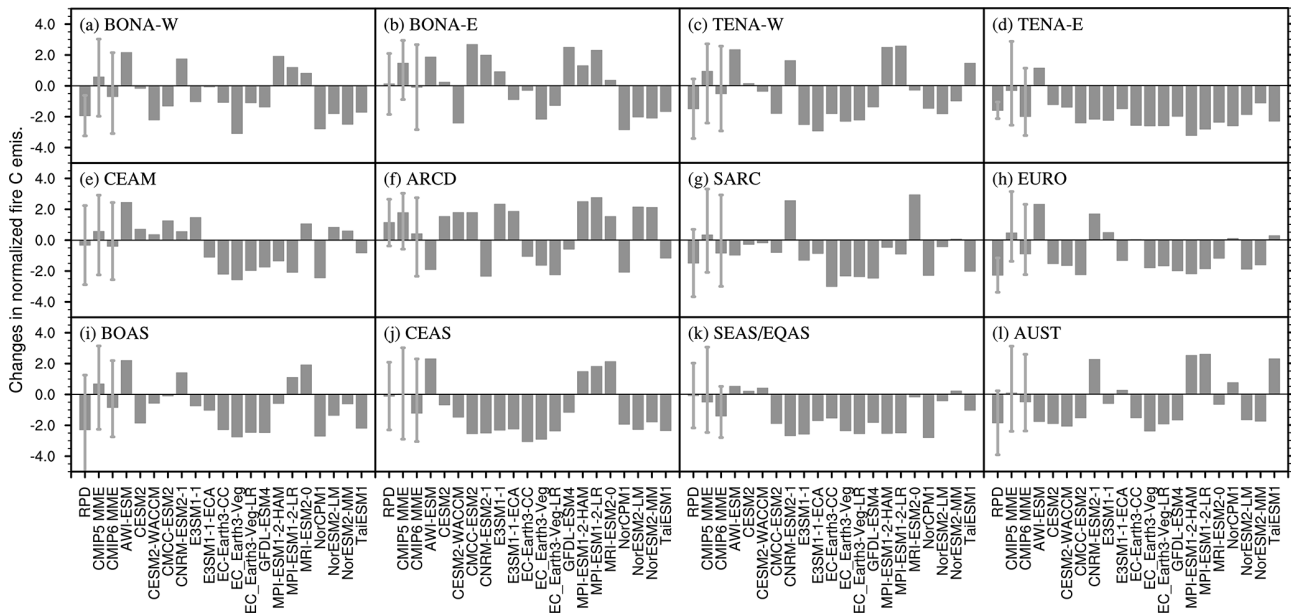


Figure 8. Comparison of normalized fire carbon emissions changes between the present-day (1985–2005) and the pre-industrial periods (1855–1875) across different sources: charcoal-based RPD, CMIP6 models, and both CMIP6 and CMIP5 MMEs. The error bars represent uncertainties, calculated as the average over the present-day and pre-industrial periods for RPD and as the range across model simulations for the MMEs.

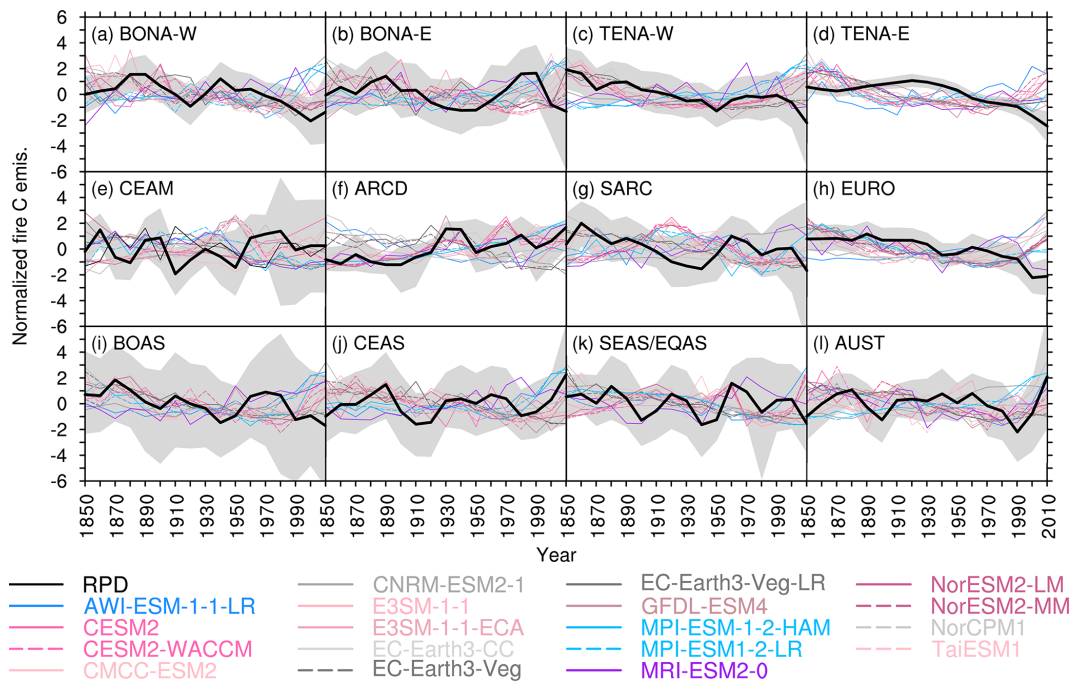


Figure 9. Standardized fire carbon emissions simulated by CMIP6 models and indicated by RPD charcoal product.

−3.8 to −2.2, and −2.2 to −1.7 Mha yr^{−2} (range of different benchmarks) for the three regions, respectively. However, CMIP6 models exhibit trends of −0.6 to 0.8, −0.3 to 0.9, and −1.5 to 0.6 Mha yr^{−2} for these regions. The failure is partly

due to the inadequate representation of human fire suppression efforts in the fire schemes (Andela et al., 2017).

Looking back to the period starting from 1850, most CMIP6 models and the CMIP6 MME simulate the change between the present day (1985–2005) and the pre-industrial

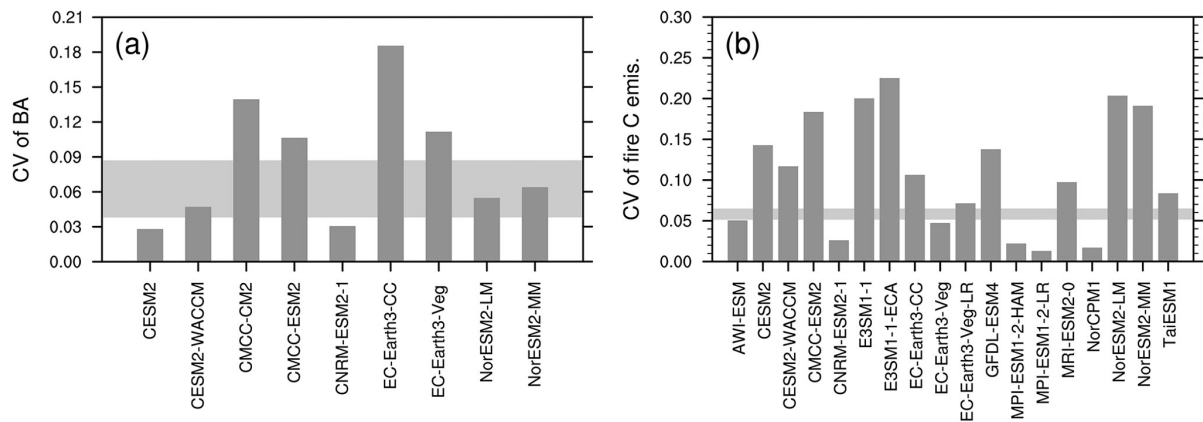


Figure 10. Same as Fig. 7 but for the coefficient of variability (CV; the standard deviation divided by the mean) of interannual variability.

period (1855–1875) that has the same sign (either an increase or decrease) as the charcoal-based reconstructions in 11 out of the 12 regions (Fig. 8). In eastern boreal North America (BONA-E), although the signs differ between the CMIP6 MME and RPD, both values are very small (Fig. 8b). In contrast, CMIP5 models show trends consistent in sign with the RPD reconstructions in only 4 of the 12 regions (BONA-E, TENA-E, ARCD, and SEAS/EQAS), indicating poorer performance compared to CMIP6 models (Fig. 8).

For time series changes, most CMIP6 models can capture the overall downward trend for 1850–1990 in western boreal North America (BONA-W), western temperate North America (TENA-W), Europe (EURO), boreal Asia (BOAS), and Australia (AUST) (Fig. 9a, c, h, i, and l) and upward trend for the arc of deforestation (ARCD) (Fig. 9f) as depicted in RPD. However, simulations and RPD have different trends in eastern temperate North America (TENA-E) and the southern arc of deforestation in South Africa (SARC) prior to the 1910s (Fig. 9d and g), as well as in temperate North America (TENA-E and TENA-W), eastern boreal North America (BONA-E), EURO, and BOAS from the 1980s onwards (Fig. 9b–d, h, and i). Since the 1980s, CMIP6 simulations have shown an increase in these regions, whereas the RPD reconstructions show a decline. The long-term (1982–2018) fire reanalysis product FireCCILT11 supports the rising trend in EURO simulated by the CMIP6 models but shows a decrease in BOAS similar to RPD (Otón et al., 2021). Furthermore, the increase in TENA-W, depicted in most CMIP6 models, is supported by the analyses of remote-sensing-based fire perimeter data sets (e.g., Abatzoglou and Kolden, 2013; Abatzoglou and Williams, 2016; Williams et al., 2019), contrary to the RPD.

Most CMIP6 models also show a decline in TENA-E fire emissions before the 1910s, while RPD and some CMIP5 models suggest an increase (Figs. 9 and S11 in the Supplement). From 1850 to 2010, the CMIP6 models using SPIT-FIRE simulate increased fire emissions in TENA-W, and

the CMIP6 models using GlobFIRM simulate decreased fire emissions in ARCD, which are not seen in the RPD reconstructions and CMIP6 models using the Li scheme (Fig. 9c and f).

3.5 Interannual variability

Unlike DGVMs that are driven by observed climate data (Li et al., 2019; Hantson et al., 2020), coupled models in CMIP are free running and driven solely by anthropogenic forcing. Consequently, they do not aim to synchronize with the actual climate state of specific years (Taylor et al., 2012; Eyring et al., 2016). Therefore, expecting a one-to-one match between CMIP-simulated and observed fires in any given year is unrealistic. Instead, we evaluate the magnitude of interannual variability and how fire activity responds to key climate drivers, such as ENSO, a dominant climate oscillation on an interannual timescale, affecting fires in the tropics (van der Werf et al., 2006; Prentice et al., 2011; Chen et al., 2017).

CMIP6 models demonstrate large inter-model discrepancies in simulating interannual variation. For burned area, the modifications of GlobFIRM implemented in CNRM-ESM2 (Delire et al., 2020) and the updates to the Li scheme employed by CESM2 and the NorESM family (Li and Lawrence, 2017) weaken interannual variation compared to EC-Earth3 and the CMCC family, respectively (Fig. 10a). For fire carbon emissions, models using the Li scheme overestimate the interannual variation, while those using SPIT-FIRE underestimate it (Fig. 10b).

The warm phase of ENSO (El Niño), characterized by warm SST anomalies in the tropical central-eastern Pacific (quantified by the Niño3.4 index), is typically initiated during the boreal summer and persists through the following spring, reaching its peak in boreal winter. Here, we assess the influence of winter (DJF) El Niño on the interannual variability of annual tropical fires averaged from the preceding June to the following May. In observations, El Niño-induced anomalies in the Walker circulation along the Equator lead to

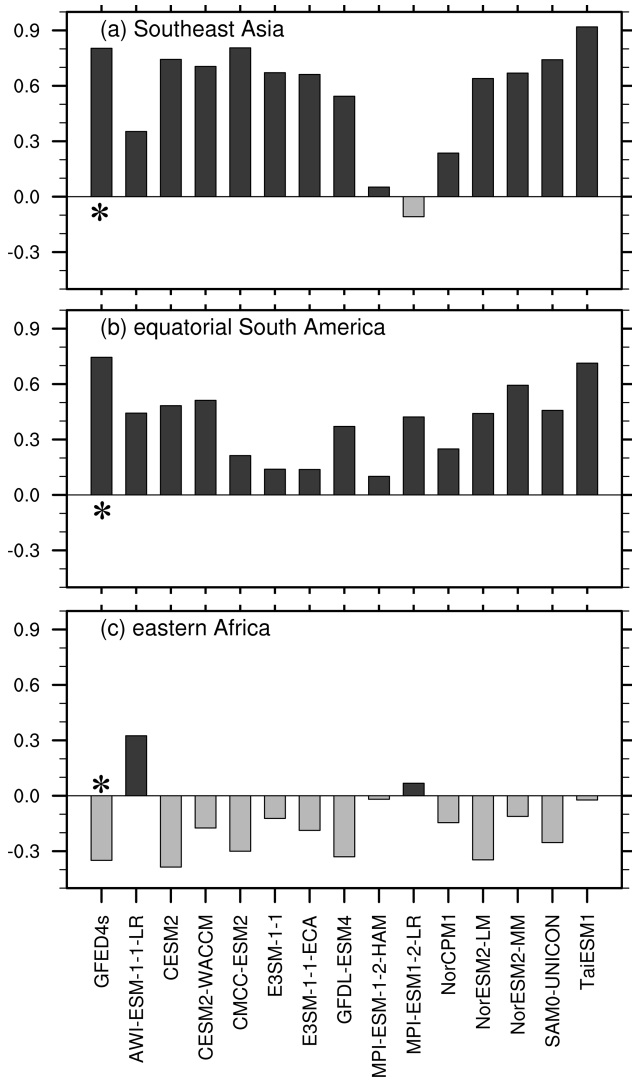


Figure 11. Correlation coefficient between the DJF Niño3.4 index and tropical fire carbon emissions averaged from the preceding June to the following May for GFED4s (1997–2019) and CMIP6 models (1850–2014). * – benchmark GFED4s. EC-Earth3 models, which only provide annual total fire emissions at the end of the year, are excluded.

decreased precipitation, increased fuel flammability, and enhanced burning and fire carbon emissions in equatorial South America and Southeast Asia, whereas they produce the opposite effect in eastern Africa (Fig. S12 in the Supplement). In general, the CMIP6 models successfully capture the response of fire carbon emissions to El Niño in the three regions, except for the models using the SPITFIRE scheme (Fig. 11). The failure of these models mainly stems from their poor simulations of the relationship between local precipitation and fire carbon emissions in Southeast Asia (i.e., mainly caused by fire model) (Fig. S13a in the Supplement) and is due to poor simulations of the relationships between both El Niño and precipitation and precipitation and fire carbon

emissions for eastern Africa and equatorial South America (Figs. S13b, c and S14b, c in the Supplement).

3.6 Relationship between fires and climatic and socioeconomic factors

Observations indicate a distinct unimodal relationship between burned area and mean annual precipitation in the tropics and subtropics (Fig. 12a): burned area increases as precipitation increases due to increased fuel load, peaking at an annual precipitation of 1100 mm yr⁻¹, and then declines as precipitation increases due to decreased fuel flammability (van der Werf et al., 2008; Archibald et al., 2009). CMIP6 models using the Li scheme reproduce the unimodal relationship, whereas models using GlobFIRM peak at an annual precipitation of 100–500 mm yr⁻¹ (Fig. 12b–j). However, all the CMIP6 models show weaker variability in magnitude than observations, indicating that the sensitivity of fires to humid conditions is underestimated.

CMIP6 models using the Li scheme outperform all CMIP5 models in reproducing the relationship between fires and wet–dry conditions. All CMIP5 models peak at lower annual precipitation values than those of the observations (Fig. S15 in the Supplement). Specifically, CESM1-BGC and CCSM4 have a maximum for mean annual precipitations of around 700–900 mm yr⁻¹, while MPI models exhibit a peak at around 400 mm yr⁻¹. Similar to CMIP6 models, all CMIP5 models underestimate the sensitivity of tropical and subtropical fires to humidity but to a greater extent (Fig. S15).

The observed burned area fraction rises with increasing population density, mainly due to increased human ignitions, peaking at 10–18 persons km⁻², and then falls due to increased human suppression (Fig. 13a) (Pechony and Shindell, 2009; Bistinas et al., 2014; Haas et al., 2022). CMIP6 models using the Li scheme and CNRM-ESM2-1 using the GlobFIRM variant reproduce the observed relationship well, while CMIP6 models using GlobFIRM and all CMIP5 models fail due to a lack of representation of human influence on fire occurrence and spread (Figs. 13b–j and S16 in the Supplement).

4 Conclusions and discussion

4.1 Summary

This study provides the first comprehensive evaluation of global fire simulations in CMIP6 ESMs and documents considerable improvements compared to CMIP5 models. Our main findings can be summarized as follows:

- *Global totals.* Most CMIP6 models, along with the multi-model ensemble mean, estimate global totals of burned area and fire carbon emissions within the range of satellite-based observations. CMIP6 addresses the major issue identified in the CMIP5 models that sim-

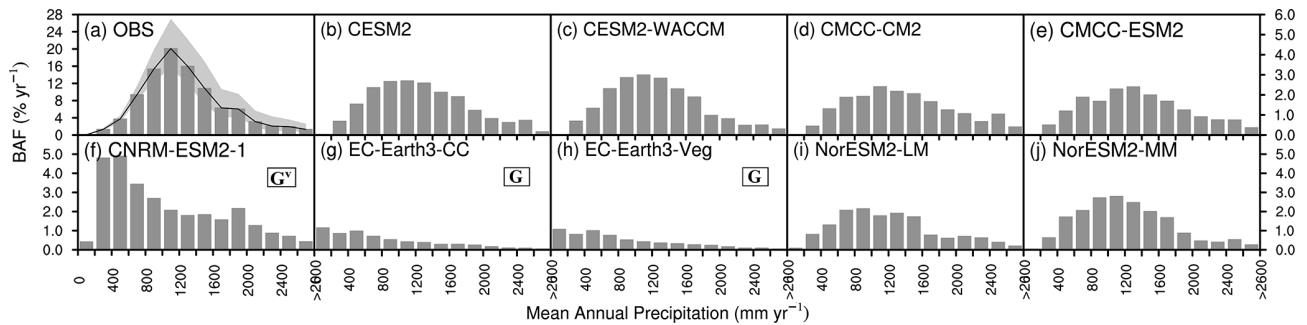


Figure 12. Burned area fraction between 35° N and 35° S in a 200 mm yr^{-1} bin of mean annual precipitation for (a) benchmarks and (b–j) CMIP6 model simulations. G and G^v denote models with GlobFIRM and its variant.

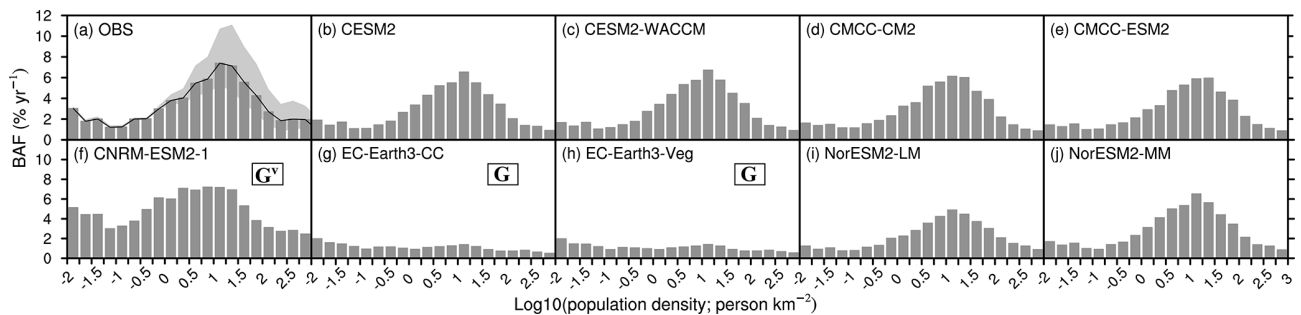


Figure 13. Burned area fraction changes with increasing population density for (a) benchmarks and (b–j) CMIP6 model simulations.

ulate a global burned area of less than half that of the observed. The increased inter-model range in CMIP6 is due to the inclusion of models using the GlobFIRM fire scheme.

- *Spatial pattern.* CMIP6 models and the ensemble mean skillfully simulate the spatial patterns of burned area and fire carbon emissions. Models using GlobFIRM have around half the skill (measured as spatial correlations) in simulating burned area compared to those using the Li scheme. Models that use the complex SPITFIRE fire scheme do not outperform the other models. Notably, CMIP6 models capture the high burned area fraction observed in Africa, whereas all CMIP5 models fail to reproduce this feature. The global correlation between the CMIP6-simulated burned area and observations is twice that of the CMIP5 models. Simulations of fire carbon emissions have been improved as well, albeit to a lesser degree.
- *Seasonal cycle.* CMIP6 models and the ensemble mean capture the major features of the fire seasonal phase (timing) but fail to reproduce the spring peak at NH mid-latitudes. They also simulated fire peak timing around 2 months later than the observed in the tropics, partly due to the bias in the simulated precipitation. Overall, CMIP6 models outperform CMIP5 models in replicating the timing. Importantly, CMIP6 addresses

the major issue identified in CMIP5 models, which simulated burned area seasonal variation (quantified using CV) at only about 30 % of the observed level.

- *Long-term trend.* CMIP6 models still fail to reproduce the observed significant decline in burned area and fire carbon emissions over the past 2 to 3 decades, largely due to an underestimation of anthropogenic influences that suppress fires. For the period 1850–2010, simulated regional changes in fire carbon emissions align with the RPD charcoal-based reconstructions, except for southern South America and eastern temperate North America before the 1910s and temperate and eastern boreal North America, Europe, and boreal Asia since the 1980s. CMIP6 simulations are generally closer to RPD than CMIP5 simulations.
- *Interannual variability.* CMIP6 models can capture the response of interannual variability of tropical fires to ENSO, except for models using the SPITFIRE fire scheme. However, there are large inter-model differences in simulating the magnitude of interannual variation.
- *Relationship of fires with precipitation and population density.* CMIP6 models capture the unimodal relationship between burned area and precipitation in the tropics and subtropics and between the global burned area and

population density, except for models using the GlobFIRM fire scheme. CMIP6 models outperform CMIP5 models, but all CMIP6 and CMIP5 models consistently underestimate fire sensitivity to precipitation.

4.2 Reasons for improved fire simulations in CMIP6

The improved fire simulations from CMIP5 to CMIP6 are mainly attributed to the development of fire schemes. The most used fire scheme has evolved to the Li scheme in CMIP6 from the GlobFIRM in CMIP5. Li et al. (2012, 2013) assessed the two schemes in CLM4 offline simulations using the same inputs (observed climate, lightning frequency, CO₂ concentration, land use and land cover change, socioeconomic conditions) and experimental design. The results indicated that the Li scheme not only aligned more closely with the observed global burned area, with estimates twice that of GlobFIRM, but also doubled the simulated skill in spatial pattern, notably capturing the high burn area fraction in Africa. Li et al. (2019), Hantson et al. (2020), and Wang et al. (2022) evaluated fire simulations of the DGVMs participating in FireMIP, which used the same protocol and input data, and confirmed the superiority of the Li scheme.

The Li fire scheme outperforms GlobFIRM primarily due to its superior core equation for calculating burned area and its calibration of parameters and functions based on observations. The Li fire scheme calculates the time-step burned area as the product of fire counts and average fire spread area per fire, in which all variables have observations, allowing for parameter calibration (Li et al., 2012, 2013). Such calibration has indeed been performed on the parameters, as documented by Li et al. (2021, 2013). GlobFIRM, on the other hand, calculates the annual burned area fraction as a nonlinear function of fire season length, where the fire season length is calculated by summing fire occurrence probability over a year (Thonicke et al., 2001). Since the probability cannot exceed 1, the burned area will be underestimated in grid cells where multiple fires occur in a time step. Furthermore, fire occurrence probability has no observations, so fire occurrence parameters cannot be calibrated. In addition, because the annual burned area is simulated, models using GloFIRM do not simulate fire seasonality. To address this, some models modified GlobFIRM to run at sub-daily to monthly time steps by using the weighted difference of running annual mean burned areas between the current and previous time steps (Krinner et al., 2005; Kloster et al., 2010; Kloster and Lasslop, 2017). However, this modification still results in a significant underestimate of seasonal variation in burned area, as shown in Fig. 6. Besides the two primary reasons, the incorporation of human influence on fires, even though partially, enhanced the simulations of the global spatial pattern of burned area.

Improvements and changes in climate simulations in CMIP6 also contribute to improved fire simulations compared to CMIP5 in some regions. The CMIP6 models reduce

the wet bias in NH Africa during the fire season (Fig. S3), resulting in higher fuel flammability and increased burned area. CMIP6 models also simulate a warmer climate in the Arctic boreal zone year-round, displaying a larger warm bias or a shift from cold bias in CMIP5 to warm bias (Fig. S4 in the Supplement). The warm bias can lead to increased vegetation growth and hence an increase in fuel availability and fuel flammability during the fire season through increased drying. Besides, CMIP6 models that incorporate the Li fire scheme simulate biomass and leaf area index (LAI) more reasonably than their model versions in CMIP5 (Danabasoglu et al., 2020; Seland et al., 2020), which contributes to more accurate estimates of fuel availability.

4.3 Implications for future fire model development

Our evaluation results indicate four critical issues in current fire models, suggesting directions for future model development.

First, CMIP6 models fail to reproduce the observed present-day significant decline in burned area and fire carbon emissions. The observed decline is largely attributed to increased human suppression (Andela et al., 2017). Archibald (2016) and Andela et al. (2017) found that the increase in land fragmentation from cropland and pasture expansion decreases fuel continuity, resulting in less burned area and lower fire emissions. Nevertheless, no fire scheme in CMIP6 ESMs parameterizes this. Furthermore, although CMIP6 ESMs using the Li scheme include parameterization on how economic development, measured by GDP per capita, enhances fire suppression, this has no impact on the CMIP6 simulations due to the GDP per capita forcing data they used being fixed at year 2000 levels. Therefore, considering the influence of landscape fragmentation on fires and using time-varying GDP per capita as forcing data could be a promising direction for future model development.

Second, CMIP6 models still underestimate the global burned area, though they are much better than CMIP5 models. The underestimation is partly because the models do not simulate multiday fires, which would allow for larger fires and thus increase the burned area. Another reason for the underestimation may be that these models calibrated their parameters and functions using older remote-sensed products. For example, the Li scheme used GFED3 (Giglio et al., 2010) for calibration (Li et al., 2012, 2013), which reports a global total burned area of around half of that indicated in the latest GFED5 product (Chen et al., 2023). Revisiting model calibrations and considering multiday fires would be helpful to improve model performance.

Third, the CMIP6 models fail to reproduce the observed spring peak in fires at NH mid-latitudes. The peak is mainly attributed to fires that occurred over croplands. While CMIP6 models using the Li scheme do simulate crop fires (Table 1), they underestimate them for two main reasons: (1) the calibration of crop fire parameters in the Li scheme was based on

GFED3 (Li et al., 2013), in which crop fires, generally classified as small fires, are much underestimated (Chen et al., 2023); (2) ESMs using the Li scheme and crop growth model (e.g., CESM family and NorESM family) assume no crop fires in managed croplands. The CMIP6 models using other fire schemes either assume that no fires occur in croplands or treat them as fires occurring in natural vegetation, leading to an underestimation or incorrect timing of crop fires. Recently, Millington et al. (2022) have deepened our understanding of fire use in croplands, detailing the varied purposes for burning, which influence the timing of burns and how environmental conditions affect these practices. Additionally, Hall et al. (2024) have developed a global cropland-focused burned area product. Incorporating the information in fire models would be a helpful step in improving model performance.

Finally, all CMIP6 models underestimate fire sensitivity to precipitation, either by increasing fuel loads as precipitation increases in more arid climates or by reducing flammability in more humid climates. This suggests the need to re-examine the parameterizations of fuel buildup and to improve the estimation of fuel wetness.

4.4 Implications for developing a reliable future fire projection product

A reliable fire projection product is crucial for knowing how fire regimes may change in the future (Pechony and Shindell, 2009; Kloster and Lasslop, 2017; Li et al., 2021; Wu et al., 2022; Yu et al., 2022). It not only aids in guiding fire management, but also is necessary for quantifying the influence of future fires on carbon, water, and energy cycles, as well as climate and human well-being (Ward et al., 2012; Jiang et al., 2016; Xie et al., 2022; Li et al., 2022; Lou et al., 2023; Park et al., 2024). Despite the clear need, such a product is currently lacking. The future fire emission forcings for CMIP6, for example, are derived from integrated assessment models (IAMs), which lack the spatial variability within a broad vegetation category (e.g., forest, grassland) across a country and the interannual variability (Feng et al., 2020). These data are not based on mechanistic models and cannot realistically represent future fire dynamics.

The CMIP6 fire simulations, based on mechanistic fire models, represent state-of-the-art multi-model source data for generating global projections of future fires. Our evaluation provides valuable insights into how to use them to produce a reliable fire protection product. Clearly, including models that perform poorly, either with respect to burned area (e.g., EC-Earth3-CC, EC-Earth3-Veg) or with respect to emissions (e.g., MRI-ESM2-0, NorCPM1), will downgrade the quality of the multi-model projection. Correcting biases in multi-year averages (van Marle et al., 2017; Lou et al., 2023), the relationship of fires with socioeconomic factors (e.g., population density, GDP per capita, road density), climatic variables (Xie et al., 2022; Yu et al., 2022), and land

cover change (Wang et al., 2023) would also improve the reliability of the projections. Finally, instead of relying on multi-model mean or median values (van Marle et al., 2017; Lou et al., 2023), it is desirable to use a weighted-average approach, in which weights are assigned based on model performance when constructing multi-model ensembles.

Code and data availability. CMIP6 and CMIP5 outputs can be accessed through the Earth System Grid Federation (ESGF) at <http://esgf-node.llnl.gov/search/cmip6/> (last access: March 2023) (Eyring et al., 2016) and <http://esgf-node.llnl.gov/search/cmip5/> (last access: March 2023) (Taylor et al., 2012), respectively. The post-processing scripts are available at <https://doi.org/10.5281/zenodo.11185326> (Li et al., 2024).

Supplement. The supplement related to this article is available online at: <https://doi.org/10.5194/gmd-17-8751-2024-supplement>.

Author contributions. FL conceived the research ideas and wrote the manuscript draft. FL, XS, and ZL conducted the evaluation analysis. XD downloaded the model outputs from the CMIP website, SPH conducted the pre-processing of the charcoal-based historical reconstruction, and FL collected other data. All authors reviewed and edited the paper.

Competing interests. At least one of the (co-)authors is a member of the editorial board of *Geoscientific Model Development*. The peer-review process was guided by an independent editor, and the authors also have no other competing interests to declare.

Disclaimer. Publisher's note: Copernicus Publications remains neutral with regard to jurisdictional claims made in the text, published maps, institutional affiliations, or any other geographical representation in this paper. While Copernicus Publications makes every effort to include appropriate place names, the final responsibility lies with the authors.

Acknowledgements. We appreciate the editor, Tatiana Egorova, for her valuable suggestions and efforts in facilitating the review process, as well as the two reviewers for their encouraging evaluation of our work and paper and their constructive comments and suggestions. We also acknowledge the World Climate Research Programme, which, through its Working Group on Coupled Modelling, coordinated and promoted CMIP5 and CMIP6. We thank the modeling groups for producing their model output and making it available, the Earth System Grid Federation (ESGF) for archiving the data and providing access, and the multiple funding agencies that support CMIP6 and ESGF.

Financial support. This study is co-supported by the National Key Research and Development Program of China (grant

no. 2022YFE0106500), the Research Council of Norway project (grant no. 328922), the Guangdong Major Project of Basic and Applied Basic Research (grant no. 2021B0301030007), and the National Science and Technology Infrastructure project Earth System Science Numerical Simulator Facility (EarthLab). This work is a contribution to the Land Ecosystem Models based On New Theory, observations and Experiments (LEMONTREE) project, funded through the generosity of Eric and Wendy Schmidt by recommendation of the Schmidt Futures program (SPH, ICP), and to the HORIZON-MSCA FIRE-ADAPT (The Role of Integrated Fire Management on Climate Change Adaptation for Ecosystem Services in Tropical and Subtropical Regions) program (SPH). L. Ruby Leung is supported by the Office of Science under the US Department of Energy's Biological and Environmental Research program through the Energy Exascale Earth System Model (E3SM) project supported by the Earth System Model Development (ESMD) program area and the HyperFACETS project supported by the Regional and Global Model Analysis (RGMA) program area. PNNL is operated under the US DOE under contract DE-AC06-76RL01830. Virginia Marécal and Roland Séférian are supported by the European Union's Horizon 2020 Research and Innovation program as part of the ESM2025 project (grant no. 101003536).

Review statement. This paper was edited by Tatiana Egorova and reviewed by two anonymous referees.

References

- Abatzoglou, J. T. and Kolden, C. A.: Relationships between climate and macroscale area burned in the western United States, *Int. J. Wildland Fire*, 22, 1003–20, <https://doi.org/10.1071/WF13019>, 2013.
- Abatzoglou, J. T. and Williams, A. P.: Impact of anthropogenic climate change on wildfire across western US forests, *P. Natl. Acad. Sci. USA*, 113, 11770–11775, <https://doi.org/10.1073/pnas.1607171113>, 2016.
- Andela, N., Morton, D. C., Giglio, L., Chen, Y., van der Werf, G. R., Kasibhatla, P. S., DeFries, R. S., Collatz, G. J., Hantson, S., Kloster, S., Bachelet, D., Forrest, M., Lasslop, G., Li, F., Manganon, S., Melton, J. R., Yue, C., and Randerson, J. T.: A human-driven decline in global burned area, *Science*, 356, 1356–1362, <https://doi.org/10.1126/science.aal4108>, 2017.
- Archibald, S.: Managing the human component of fire regimes: lessons from Africa, *Philos. T. R. Soc. B*, 371, 20150346, <https://doi.org/10.1098/rstb.2015.0346>, 2016.
- Archibald, S., Roy, D. P., van Wilgen, B. W., and Scholes, R. J.: What limits fire? An examination of drivers of burnt area in Southern Africa, *Glob. Change Biol.*, 15, 613–630, <https://doi.org/10.1111/j.1365-2486.2008.01754.x>, 2009.
- Bayley, G. V. and Hammersley, J. M.: The “effective” number of independent observations in an autocorrelated time series, *J. R. Stat. Soc.*, 8, 184–197, <https://doi.org/10.2307/2983560>, 1946.
- Bethke, I., Wang, Y., Counillon, F., Keenlyside, N., Kimmritz, M., Fransner, F., Samuelsen, A., Langehaug, H., Svendsen, L., Chiu, P.-G., Passos, L., Bentsen, M., Guo, C., Gupta, A., Tjiputra, J., Kirkevåg, A., Olivé, D., Seland, Ø., Solsvik Vågane, J., Fan, Y., and Eldevik, T.: NorCPM1 and its contribution to CMIP6 DCP, *Geosci. Model Dev.*, 14, 7073–7116, <https://doi.org/10.5194/gmd-14-7073-2021>, 2021.
- Bistinas, I., Harrison, S. P., Prentice, I. C., and Pereira, J. M. C.: Causal relationships versus emergent patterns in the global controls of fire frequency, *Biogeosciences*, 11, 5087–5101, <https://doi.org/10.5194/bg-11-5087-2014>, 2014.
- Bowman, D. M. J. S., Balch, J. K., Artaxo, P., Bond, W. J., Carlson, J. M., Cochrane, M. A., D'Antonio, C. M., DeFries, R. S., Doyle, J. C., Harrison, S. P., Johnston, F. H., Keeley, J. E., Krawchuk, M. A., Kull, C. A., Marston, J. B., Moritz, M. A., Prentice, I. C., Roos, C. I., Scott, A. C., Swetnam, T. W., van der Werf, G. R., and Pyne, S. J.: Fire in the Earth system, *Science*, 324, 481–484, <https://doi.org/10.1126/science.1163886>, 2009.
- Bond-Lamberty, B., Peckham, S. D., Ahl, D. E., and Gower, S. T.: Fire as the dominant driver of central Canadian boreal forest carbon balance, *Nature*, 450, 89–92, <https://doi.org/10.1038/nature06272>, 2007.
- Burrows, S. M., Maltrud, M., Yang, X., Zhu, Q., Jeffery, N., Shi, X., Ricciuto, D., Wang, S., Bisht, G., Tang, J., Wolfe, J., Harrop, B. E., Singh, B., Brent, L., Baldwin, S., Zhou, T., Cameron-Smith, P., Keen, N., Collier, N., Xu, M., Hunke, E. C., Elliott, S. M., Turner, A. K., Li, H., Wang, H., Golaz, J. C., Bond-Lamberty, B., Hoffman, F. M., Riley, W. J., Thornton, P. E., Calvin, K., and Leung, L. R.: The DOE E3SM v1.1 biogeochemistry configuration: Description and simulated ecosystem-climate responses to historical changes in forcing, *J. Adv. Model. Earth Sy.*, 12, e2019MS001766, <https://doi.org/10.1029/2019MS001766>, 2020.
- Chen, Y., Morton, D. C., Andela, N., van der Werf, G. R., Giglio, L., and Randerson, J. T.: A pan-tropical cascade of fire driven by El Niño/Southern Oscillation, *Nat. Clim. Change*, 7, 906–911, <https://doi.org/10.1038/s41558-017-0014-8>, 2017.
- Chen, Y., Hall, J., van Wees, D., Andela, N., Hantson, S., Giglio, L., van der Werf, G. R., Morton, D. C., and Randerson, J. T.: Multi-decadal trends and variability in burned area from the fifth version of the Global Fire Emissions Database (GFED5), *Earth Syst. Sci. Data*, 15, 5227–5259, <https://doi.org/10.5194/essd-15-5227-2023>, 2023.
- Cherchi, A., Fogli, P. G., Lovato, T., Peano, D., Iovino, D., Gualdi, S., Masina, S., Scoccimarro, E., Matera, S., Bellucci, A., and Navarra, A.: Global mean climate and main patterns of variability in the CMCC-CM2 coupled model, *J. Adv. Model. Earth Sy.*, 11, 185–209, <https://doi.org/10.1029/2018MS001369>, 2019.
- Chuvieco, E., Pettinari, M. L., Bastarrika, A., Roteta, E., Storm, T., and Padilla Parellada, M.: ESA Fire Climate Change Initiative (Fire_cci): Small Fire Dataset (SFD) Burned Area pixel product for Sub-Saharan Africa (version 1.1), Centre for Environmental Data Analysis [data set], <https://doi.org/10.5285/065f6040ef08485db989cbd89d536167>, 2018.
- Clifford, P., Richardson, S., and Hémon, D.: Assessing the significance of the correlation between two spatial processes, *Biometrics*, 45, 123–134, <https://doi.org/10.2307/2532039>, 1989.
- Contzen, J., Dickhaus, T., and Lohmann, G.: Variability and extremes: statistical validation of the Alfred Wegener Institute Earth System Model (AWI-ESM), *Geosci. Model Dev.*, 15, 1803–1820, <https://doi.org/10.5194/gmd-15-1803-2022>, 2022.
- Danabasoglu, G., Lamarque, J.-F., Bacmeister, J., Bailey, D. A., DuVivier, A. K., Edwards, J., Emmons, L. K., Fasullo, J., Gar-

- cia, R., Gettelman, A., Hannay, C., Holland, M. M., Large, W. G., Lauritzen, P. H., Lawrence, D. M., Lenaerts, J. T. M., Lindsay, K., Lipscomb, W. H., Mills, M. J., Neale, R., Oleson, K. W., Otto-Bliessner, B., Phillips, A. S., Sacks, W., Tilmes, S., van Kampenhout, L., Vertenstein, M., Bertini, A., Dennis, J., Deser, C., Fischer, C., Fox-Kemper, B., Kay, J. E., Kinnison, D., Kushner, P. J., Larson, V. E., Long, M. C., Mickelson, S., Moore, J. K., Nienhouse, E., Polvani, L., Rasch, P. J., and Strand, W. G.: The Community Earth System Model Version 2 (CESM2), *J. Adv. Model. Earth Sy.*, 12, e2019MS001916, <https://doi.org/10.1029/2019MS001916>, 2020.
- Delire, C., Séférian, R., Decharme, B., Alkama, R., Calvet, J.-C., Carrer, D., Gibelin, A.-L., Joetzjer, E., Morel, X., Rocher, M., and Diane Tzanos, D.: The global land carbon cycle simulated with ISBA-CTrip: Improvements over the last decade, *J. Adv. Model. Earth Sy.*, 12, e2019MS001886, <https://doi.org/10.1029/2019MS001886>, 2020.
- Döscher, R., Acosta, M., Alessandri, A., Anthoni, P., Arsouze, T., Bergman, T., Bernardello, R., Boussetta, S., Caron, L.-P., Carver, G., Castrillo, M., Catalano, F., Cvijanovic, I., Davini, P., Dekker, E., Doblus-Reyes, F. J., Docquier, D., Echevarria, P., Fladrich, U., Fuentes-Franco, R., Gröger, M., v. Hardenberg, J., Hieronymus, J., Karami, M. P., Keskinen, J.-P., Koenigk, T., Makkonen, R., Massonnet, F., Ménégos, M., Miller, P. A., Moreno-Chamarro, E., Nieradzik, L., van Noije, T., Nolan, P., O'Donnell, D., Olinaho, P., van den Oord, G., Ortega, P., Prims, O. T., Ramos, A., Reerink, T., Rousset, C., Ruprich-Robert, Y., Le Sager, P., Schmith, T., Schrödner, R., Serva, F., Sicardi, V., Sloth Madssen, M., Smith, B., Tian, T., Tourigny, E., Uotila, P., Vancoppenolle, M., Wang, S., Wårlind, D., Willén, U., Wyser, K., Yang, S., Yepes-Arbós, X., and Zhang, Q.: The EC-Earth3 Earth system model for the Coupled Model Intercomparison Project 6, *Geosci. Model Dev.*, 15, 2973–3020, <https://doi.org/10.5194/gmd-15-2973-2022>, 2022.
- Dunne, J. P., Horowitz, L. W., Adcroft, A. J., Ginoux, P., Held, I. M., John, J. G., Krasting, J. P., Malyshev, S., Naik, V., Paulot, F., Shevliakova, E., Stock, C. A., Zadeh, N., Balaji, V., Blanton, C., Dunne, K. A., Dupuis, C., Durachta, J., Dussin, R., Gauthier, P. P. G., Griffies, S. M., Guo, H., Hallberg, R. W., Harrison, M., He, J., Hurlin, W., McHugh, C., Menzel, R., Milly, P. C. D., Nikonov, S., Paynter, D. J., Ploshay, J., Radhakrishnan, A., Rand, K., Reichl, B. G., Robinson, T., Schwarzkopf, D. M., Sentman, L. T., Underwood, S., Vahlenkamp, H., Winton, M., Wittenberg, A. T., Wyman, B., Zeng, Y., and Zhao, M.: The GFDL Earth System Model Version 4.1 (GFDL-ESM 4.1): Overall Coupled Model Description and Simulation Characteristics, *J. Adv. Model. Earth Sy.*, 12, e2019MS002015, <https://doi.org/10.1029/2019MS002015>, 2020.
- Eyring, V., Bony, S., Meehl, G. A., Senior, C. A., Stevens, B., Stouffer, R. J., and Taylor, K. E.: Overview of the Coupled Model Intercomparison Project Phase 6 (CMIP6) experimental design and organization, *Geosci. Model Dev.*, 9, 1937–1958, <https://doi.org/10.5194/gmd-9-1937-2016>, 2016 (data available at: <http://esgf-node.llnl.gov/search/cmip6/>, last access: March 2023).
- Feng, L., Smith, S. J., Braun, C., Crippa, M., Gidden, M. J., Hoesly, R., Klimont, Z., van Marle, M., van den Berg, M., and van der Werf, G. R.: The generation of gridded emissions data for CMIP6, *Geosci. Model Dev.*, 13, 461–482, <https://doi.org/10.5194/gmd-13-461-2020>, 2020.
- Giglio, L., Boschetti, L., Roy, D. P., Humber, M. L., and Justice, C. O.: The Collection 6 MODIS burned area mapping algorithm and product, *Remote Sens. Environ.*, 217, 72–85, <https://doi.org/10.1016/j.rse.2018.08.005>, 2018.
- Haas, O., Prentice, I. C., and Harrison, S. P.: Global environmental controls on wildfire burnt area, size and intensity, *Environ. Res. Lett.*, 17, 065004, <https://doi.org/10.1088/1748-9326/ac6a69>, 2022.
- Hall, J. V., Argueta, F., Zubkova, M., Chen, Y., Randerson, J. T., and Giglio, L.: GloCAB: global cropland burned area from mid-2002 to 2020, *Earth Syst. Sci. Data*, 16, 867–885, <https://doi.org/10.5194/essd-16-867-2024>, 2024.
- Hanson, S., Kelley, D. L., Arneeth, A., Harrison, S. P., Archibald, S., Bachelet, D., Forrest, M., Hickler, T., Lasslop, G., Li, F., Mangeon, S., Melton, J. R., Nieradzik, L., Rabin, S. S., Prentice, I. C., Sheehan, T., Sitch, S., Teckentrup, L., Voulgarakis, A., and Yue, C.: Quantitative assessment of fire and vegetation properties in simulations with fire-enabled vegetation models from the Fire Model Intercomparison Project, *Geosci. Model Dev.*, 13, 3299–3318, <https://doi.org/10.5194/gmd-13-3299-2020>, 2020.
- Harris, I., Osborn, T. J., Jones, P., and Lister, D.: Version 4 of the CRU TS monthly high-resolution gridded multivariate climate dataset, *Sci. Data*, 7, 109, <https://doi.org/10.1038/s41597-020-0453-3>, 2020.
- Harrison, S. P., Villegas-Diaz, R., Cruz-Silva, E., Gallagher, D., Kesner, D., Lincoln, P., Shen, Y., Sweeney, L., Colombaroli, D., Ali, A., Barhoumi, C., Bergeron, Y., Blyakharchuk, T., Bobek, P., Bradshaw, R., Clear, J. L., Czerwiński, S., Daniau, A.-L., Dodson, J., Edwards, K. J., Edwards, M. E., Feurdean, A., Foster, D., Gajewski, K., Gałka, M., Garneau, M., Giesecke, T., Gil Romera, G., Girardin, M. P., Hofer, D., Huang, K., Inoue, J., Jamrichová, E., Jasiunas, N., Jiang, W., Jiménez-Moreno, G., Karpińska-Kotaczek, M., Kotaczek, P., Kuosmanen, N., Lamentowicz, M., Lavoie, M., Li, F., Li, J., Lisitsyna, O., López-Sáez, J. A., Luélmo-Lautenschlaeger, R., Magnan, G., Magyari, E. K., Maksims, A., Marcisz, K., Marinova, E., Marlon, J., Mensing, S., Miroslaw-Grabowska, J., Oswald, W., Pérez-Díaz, S., Pérez-Obiol, R., Piilo, S., Poska, A., Qin, X., Remy, C. C., Richard, P. J. H., Salonen, S., Sasaki, N., Schneider, H., Shoytk, W., Stancikaite, M., Šteinberga, D., Stivrins, N., Takahara, H., Tan, Z., Trasune, L., Umbanhowar, C. E., Väliaranta, M., Vassiljev, J., Xiao, X., Xu, Q., Xu, X., Zawisza, E., Zhao, Y., Zhou, Z., and Paillard, J.: The Reading Palaeofire Database: an expanded global resource to document changes in fire regimes from sedimentary charcoal records, *Earth Syst. Sci. Data*, 14, 1109–1124, <https://doi.org/10.5194/essd-14-1109-2022>, 2022.
- Hurt, G. C., Chini, L., Sahajpal, R., Frolking, S., Bodirsky, B. L., Calvin, K., Doelman, J. C., Fisk, J., Fujimori, S., Klein Goldewijk, K., Hasegawa, T., Havlik, P., Heinemann, A., Humpenöder, F., Jungclaus, J., Kaplan, J. O., Kennedy, J., Krisztin, T., Lawrence, D., Lawrence, P., Ma, L., Mertz, O., Pongratz, J., Popp, A., Poulter, B., Riahi, K., Shevliakova, E., Stehfest, E., Thornton, P., Tubiello, F. N., van Vuuren, D. P., and Zhang, X.: Harmonization of global land use change and management for the period 850–2100 (LUH2) for CMIP6, *Geosci. Model Dev.*, 13, 5425–5464, <https://doi.org/10.5194/gmd-13-5425-2020>, 2020.

- Ichoku, C. and Ellison, L.: Global top-down smoke-aerosol emissions estimation using satellite fire radiative power measurements, *Atmos. Chem. Phys.*, 14, 6643–6667, <https://doi.org/10.5194/acp-14-6643-2014>, 2014.
- IPCC: Climate Change 2021: The Physical Science Basis. Contribution of Working Group I to the Sixth Assessment Report of the Intergovernmental Panel on Climate Change, edited by: Masson-Delmotte, V., Zhai, P., Pirani, A., Connors, S. L., Péan, C., Berger, S., Caud, N., Chen, Y., Goldfarb, L., Gomis, M. I., Huang, M., Leitzell, K., Lonnoy, E., Matthews, J. B. R., Maycock, T. K., Waterfield, T., Yelekçi, O., Yu, R., and Zhou, B., Cambridge University Press, Cambridge, United Kingdom and New York, NY, USA, 2391 pp., 2021.
- Jiang, Y., Lu, Z., Liu, X., Qian, Y., Zhang, K., Wang, Y., and Yang, X.-Q.: Impacts of global open-fire aerosols on direct radiative, cloud and surface-albedo effects simulated with CAM5, *Atmos. Chem. Phys.*, 16, 14805–14824, <https://doi.org/10.5194/acp-16-14805-2016>, 2016.
- Kaiser, J. W., Heil, A., Andreae, M. O., Benedetti, A., Chubarova, N., Jones, L., Morcrette, J.-J., Razinger, M., Schultz, M. G., Suttie, M., and van der Werf, G. R.: Biomass burning emissions estimated with a global fire assimilation system based on observed fire radiative power, *Biogeosciences*, 9, 527–554, <https://doi.org/10.5194/bg-9-527-2012>, 2012.
- Kim, J.-S., Kug, J.-S., Jeong, S.-J., Park, H., and Schaepman-Strub, G.: Extensive fires in southeastern Siberian permafrost linked to preceding Arctic Oscillation, *Science Advances*, 6, eaax3308, <https://doi.org/10.1126/sciadv.aax3308>, 2020.
- Klein Goldewijk, K., Beusen, A., Doelman, J., and Stehfest, E.: Anthropogenic land use estimates for the Holocene – HYDE 3.2, *Earth Syst. Sci. Data*, 9, 927–953, <https://doi.org/10.5194/essd-9-927-2017>, 2017.
- Kloster, S. and Lasslop, G.: Historical and future fire occurrence (1850 to 2100) simulated in CMIP5 Earth System Models, *Global Planet. Change*, 150, 58–69, <https://doi.org/10.1016/j.gloplacha.2016.12.017>, 2017.
- Kloster, S., Mahowald, N. M., Randerson, J. T., Thornton, P. E., Hoffman, F. M., Levis, S., Lawrence, P. J., Feddes, J. J., Oleson, K. W., and Lawrence, D. M.: Fire dynamics during the 20th century simulated by the Community Land Model, *Biogeosciences*, 7, 1877–1902, <https://doi.org/10.5194/bg-7-1877-2010>, 2010.
- Krinner, G., Viovy, N., de Noblet-Ducoudré, N., Ogée, J., Polcher, J., Friedlingstein, P., Ciais, P., Sitch, S., and Prentice, I. C.: A dynamic global vegetation model for studies of the coupled atmosphere-biosphere system, *Global Biogeochem. Cy.*, 19, 1–33, <https://doi.org/10.1029/2003GB002199>, 2005.
- Lasslop, G., Thonicke, K., and Kloster, S.: SPITFIRE within the MPI Earth system model: Model development and evaluation, *J. Adv. Model Earth Sy.*, 6, 740–755, <https://doi.org/10.1002/2013MS000284>, 2014.
- Lasslop, G., Hantson, S., Harrison, S. P., Bachelet, D., Burton, C., Forkel, M., Forrest, M., Li F., Melton, J. R., Yue, C., Archibald, S., Scheiter, S., Arneth, A., Hickler, T., and Sitch, S.: Global ecosystems and fire: Multi-model assessment of fire-induced tree-cover and carbon storage reduction, *Glob. Change Biol.*, 26, 5027–5041, <https://doi.org/10.1111/gcb.15160>, 2020.
- Lee, W.-L., Wang, Y.-C., Shiu, C.-J., Tsai, I., Tu, C.-Y., Lan, Y.-Y., Chen, J.-P., Pan, H.-L., and Hsu, H.-H.: Taiwan Earth System Model Version 1: description and evaluation of mean state, *Geosci. Model Dev.*, 13, 3887–3904, <https://doi.org/10.5194/gmd-13-3887-2020>, 2020.
- Li, F. and Lawrence, D. M.: Role of fire in the global land water budget during the 20th century through changing ecosystems, *J. Climate*, 30, 1893–908, <https://doi.org/10.1175/JCLI-D-16-0460.1>, 2017.
- Li, F., Zeng, X. D., and Levis, S.: A process-based fire parameterization of intermediate complexity in a Dynamic Global Vegetation Model, *Biogeosciences*, 9, 2761–2780, <https://doi.org/10.5194/bg-9-2761-2012>, 2012.
- Li, F., Levis, S., and Ward, D. S.: Quantifying the role of fire in the Earth system – Part 1: Improved global fire modeling in the Community Earth System Model (CESM1), *Biogeosciences*, 10, 2293–2314, <https://doi.org/10.5194/bg-10-2293-2013>, 2013.
- Li, F., Lawrence, D. M., and Bond-Lamberty, B.: Impact of fire on global land surface air temperature and energy budget for the 20th century due to changes within ecosystems, *Environ. Res. Lett.*, 12, 044014, <https://doi.org/10.1088/1748-9326/aa6685>, 2017.
- Li, F., Lawrence, D. M., and Bond-Lamberty, B.: Human impacts on 20th century fire dynamics and implications for global carbon and water trajectories, *Global Planet. Change*, 162, 18–27, <https://doi.org/10.1016/j.gloplacha.2018.01.002>, 2018.
- Li, F., Val Martin, M., Andreae, M. O., Arneth, A., Hantson, S., Kaiser, J. W., Lasslop, G., Yue, C., Bachelet, D., Forrest, M., Kluzek, E., Liu, X., Mangeon, S., Melton, J. R., Ward, D. S., Darnenov, A., Hickler, T., Ichoku, C., Magi, B. I., Sitch, S., van der Werf, G. R., Wiedinmyer, C., and Rabin, S. S.: Historical (1700–2012) global multi-model estimates of the fire emissions from the Fire Modeling Intercomparison Project (FireMIP), *Atmos. Chem. Phys.*, 19, 12545–12567, <https://doi.org/10.5194/acp-19-12545-2019>, 2019.
- Li, F., Lawrence, D. M., Jiang, Y., Liu, X., and Lin, Z.: Fire aerosols slow down the global water cycle, *J. Climate*, 35, 3619–3633, <https://doi.org/10.1175/JCLI-D-21-0817.1>, 2022.
- Li, F., Song, X., Lin, Z., and Harrison, S. P.: Post-processing scripts for gmd-2024-85, Zenodo [code], <https://doi.org/10.5281/zenodo.11185326>, 2024.
- Lou, S., Liu, Y., Bai, Y., Li, F., Lin, G., Xu, L., Liu, Z., Chen, Y., Dong, X., Zhao, M., Wang, L., Jin, M., Wang, C., Cai, W., Gong, P., and Luo, Y.: Projections of mortality risk attributable to short-term exposure to landscape fire smoke in China, 2021–2100: A health impact assessment study, *Lancet Planet. Heal.*, 7, e841–e849, [https://doi.org/10.1016/S2542-5196\(23\)00192-4](https://doi.org/10.1016/S2542-5196(23)00192-4), 2023.
- Lovato, T., Peano, D., Butenschön, M., Matera, S., Iovino, D., Scoccimarro, E., Fogli, P. G., Cherchi, A., Bellucci, A., Gualdi, S., and Masina, S.: CMIP6 Simulations with the CMCC Earth System Model (CMCC-ESM2), *J. Adv. Model Earth Sy.*, 14, p.e2021MS002814, <https://doi.org/10.1029/2021MS002814>, 2022.
- Mauritsen, T., Bader, J., Becker, T., Behrens, J., Bittner, M., Brokopf, R., Brovkin, V., Claussen, M., Crueger, T., Esch, M., Fast, I., Fiedler, S., Fläschner, D., Gayler, V., Giorgetta, M., Goll, D. S., Haak, H., Hagemann, S., Hedemann, C., Hohenegger, C., Ilyina, T., Jahns, T., Jimenez-de-la-Cuesta, D., Jungclaus, J., Kleinen, T., Kloster, S., Kracher, D., Kinne, S., Kleberg, D., Lasslop, G., Kornbluh, L., Marotzke, J., Matei, D., Meraner, K., Mikolajewicz, U., Modali, K., Möbis, B., Müller, W. A., Nabel,

- J. E. M. S., Nam, C. C. W., Notz, D., Nyawira, S.-S., Paulsen, H., Peters, K., Pincus, R., Pohlmann, H., Pongratz, J., Popp, M., Raddatz, T. J., Rast, S., Redler, R., Reick, C. H., Rohrschneider, T., Schemann, V., Schmidt, H., Schnur, R., Schulzweida, U., Six, K. D., Stein, L., Stemmler, I., Stevens, B., von Storch, J.-S., Tian, F., Voigt, A., Vrese, P., Wieners, K.-H., Wilken-skjeld, S., Winkler, A., and Roeckner, E.: Developments in the MPIM Earth System Model version 1.2 (MPI-ESM1.2) and its response to increasing CO₂, *J. Adv. Model. Earth Sy.*, 11, 998–1038, <https://doi.org/10.1029/2018MS001400>, 2019.
- Meinshausen, M., Vogel, E., Nauels, A., Lorbacher, K., Meinshausen, N., Etheridge, D. M., Fraser, P. J., Montzka, S. A., Rayner, P. J., Trudinger, C. M., Krummel, P. B., Beyerle, U., Canadell, J. G., Daniel, J. S., Enting, I. G., Law, R. M., Lunder, C. R., O'Doherty, S., Prinn, R. G., Reimann, S., Rubino, M., Velders, G. J. M., Vollmer, M. K., Wang, R. H. J., and Weiss, R.: Historical greenhouse gas concentrations for climate modelling (CMIP6), *Geosci. Model Dev.*, 10, 2057–2116, <https://doi.org/10.5194/gmd-10-2057-2017>, 2017.
- Millington, J. D., Perkins, O., and Smith, C.: Human fire use and management: a global database of anthropogenic fire impacts for modelling, *Fire*, 5, 87, <https://doi.org/10.3390/fire5040087>, 2022.
- Neubauer, D., Ferrachat, S., Siegenthaler-Le Drian, C., Stoll, J., Folini, D. S., Tegen, I., Wieners, K. H., Mauritsen, T., Stemmler, I., Barthel, S., Bey, I., Daskalakis, N., Heinold, B., Kokkola, H., Partridge, D., Rast, S., Schmidt, H., Schutgens, N., Stanelle, T., Stier, P., Watson-Parris, D., and Lohmann, U.: HAMMOZ-Consortium MPI-ESM1. 2-HAM model output prepared for CMIP6 CMIP historical, Version 20201101, [data set], Earth System Grid Federation, <https://doi.org/10.22033/ESGF/CMIP6.1622>, 2019.
- Otón, G., Pereira, J. M. C., Silva, J. M. N., and Chuvieco, E.: Analysis of Trends in the FireCCI Global Long Term Burned Area Product (1982–2018), *Fire*, 4, 74, <https://doi.org/10.3390/fire4040074>, 2021.
- Park, C., Takahashi, K., Fujimori, S., Phung, V., Li, F., Takakura, J., Hasegawa, T., and Jansakoo, T.: Future fire-PM_{2.5} mortality varies depending on climate and socioeconomic changes, *Environ. Res. Lett.*, 19, 024003, <https://doi.org/10.1088/1748-9326/ad1b7d>, 2024.
- Pechony, O. and Shindell, D. T.: Fire parameterization on a global scale, *J. Geophys. Res.*, 114, D16115, <https://doi.org/10.1029/2009JD011927>, 2009.
- Power, M. J., Marlon, J. R., Bartlein, P. J., and Harrison, S. P.: Fire history and the Global Charcoal Database: a new tool for hypothesis testing and data exploration, *Palaeogeogr. Palaeoclimatol.*, 291, 52–59, <https://doi.org/10.1016/j.palaeo.2009.09.014>, 2010.
- Prentice, I. C., Kelley, D. I., Foster, P. N., Friedlingstein, P., Harrison, S. P., and Bartlein, P. J.: Modeling fire and the terrestrial carbon balance, *Global Biogeochem. Cy.*, 25, GB3005, <https://doi.org/10.1029/2010GB003906>, 2011.
- Rabin, S. S., Ward, D. S., Malyshev, S. L., Magi, B. I., Shevliakova, E., and Pacala, S. W.: A fire model with distinct crop, pasture, and non-agricultural burning: use of new data and a model-fitting algorithm for FINAL.1, *Geosci. Model Dev.*, 11, 815–842, <https://doi.org/10.5194/gmd-11-815-2018>, 2018.
- Randerson, J. T., Liu, H., Flanner, M. G., Chambers, S. D., Jin, Y., Hess, P. G., Pfister, G., Mack, M. C., Treseder, K. K., and Welp, L. R.: The impact of boreal forest fire on climate warming, *Science*, 314, 1130–1132, <https://doi.org/10.1126/science.1132075>, 2006.
- Rayner, N. A., Parker, D. E., Horton, E. B., Folland, C. K., Alexander, L. V., Rowell, D. P., Kent, E. C., and Kaplan, A.: Global analyses of sea surface temperature, sea ice, and night marine air temperature since the late nineteenth century, *J. Geophys. Res.*, 108, 4407, <https://doi.org/10.1029/2002JD002670>, 2003.
- Scholze, M., Allen, J. I., Collins, W. J., Cornell, S. E., Huntingford, C., Joshi, M., Lowe, J. A., Smith, R. S., and Wild, O.: Earth system models: a tool to understand changes in the Earth system, in: *Understanding the Earth System. Global Change Science for Applications*, edited by: Cornell, S. E., Prentice, I. C., House, J. I., and Downy, C. J., Cambridge University Press, Cambridge, 129–159, 2013.
- Scott, A. C. and Glasspool, I. J.: The diversification of Palaeozoic fire systems and fluctuations in atmospheric oxygen concentration, *P. Natl. Acad. Sci. USA*, 103, 10861–10865, <https://doi.org/10.1073/pnas.0604090103>, 2006.
- Séférian, R., Nabat, P., Michou, M., Saint-Martin, D., Voldoire, A., Colin, J., Decharme, B., Delire, C., Berthet, S., Chevallier, M., Sénési, S., Franchisteguy, L., Vial, J., Mallet, M., Joetzjer, E., Geoffroy, O., Guérémy, J. F., Moine, M. P., Msadek, R., Ribes, A., Rocher, M., Roehrig, R., Salas-y-Méla, D., Sanchez, E., Terray, L., Valcke, L., Waldman, R., Aumont, O., Bopp, L., Deshayes, J., Été, C., and Madec, G.: Evaluation of CNRM Earth System Model, CNRM-ESM2-1: Role of Earth system processes in present-day and future climate, *J. Adv. Model. Earth Sy.*, 11, 4182–4227, <https://doi.org/10.1029/2019MS001791>, 2019.
- Seland, Ø., Bentsen, M., Olivieri, D., Toniazzo, T., Gjermundsen, A., Graff, L. S., Debernard, J. B., Gupta, A. K., He, Y.-C., Kirkevåg, A., Schwinger, J., Tjiputra, J., Aas, K. S., Bethke, I., Fan, Y., Griesfeller, J., Grini, A., Guo, C., Ilicak, M., Karset, I. H. H., Landgren, O., Liakka, J., Moseid, K. O., Nummelin, A., Spensberger, C., Tang, H., Zhang, Z., Heinze, C., Iversen, T., and Schulz, M.: Overview of the Norwegian Earth System Model (NorESM2) and key climate response of CMIP6 DECK, historical, and scenario simulations, *Geosci. Model Dev.*, 13, 6165–6200, <https://doi.org/10.5194/gmd-13-6165-2020>, 2020.
- Song, X., Wang, D.-Y., Li, F., and Zeng, X.-D.: Evaluating the performance of CMIP6 Earth system models in simulating global vegetation structure and distribution, *Adv. Climate Change Res.*, 12, 584–595, <https://doi.org/10.1016/j.accre.2021.06.008>, 2021.
- Taylor, K. E., Stouffer, R. J., and Meehl, G. A.: An Overview of Cmpip5 and the Experiment Design, *B. Am. Meteorol. Soc.*, 93, 485–498, <https://doi.org/10.1175/Bams-D-11-00094.1>, 2012 (data available at: <http://esgf-node.llnl.gov/search/cmip5/>, last access: March 2023).
- Thonicke, K., Venevsky, S., Sitch, S., and Cramer, W.: The role of fire disturbance for global vegetation dynamics: Coupling fire into a Dynamic Global Vegetation Model, *Global Ecol. Biogeogr.*, 10, 661–677, <https://doi.org/10.1046/j.1466-822X.2001.00175.x>, 2001.
- Thonicke, K., Spessa, A., Prentice, I. C., Harrison, S. P., Dong, L., and Carmona-Moreno, C.: The influence of vegetation, fire spread and fire behaviour on biomass burning and trace gas emissions: results from a process-based model, *Biogeosciences*, 7, 1991–2011, <https://doi.org/10.5194/bg-7-1991-2010>, 2010.

- United Nations Environment Programme (UNEP): Spreading like Wildfire – The Rising Threat of Extraordinary Landscape Fires, A UNEP Rapid Response Assessment, Nairobi, <https://www.unep.org/resources/report/spreading-wildfire-rising-threat-extraordinary-landscape-fires> (last access: March 2023), 126 pp., 2022.
- van Marle, M. J. E., Kloster, S., Magi, B. I., Marlon, J. R., Daniou, A.-L., Field, R. D., Arneeth, A., Forrest, M., Hantson, S., Kehrwald, N. M., Knorr, W., Lasslop, G., Li, F., Manguon, S., Yue, C., Kaiser, J. W., and van der Werf, G. R.: Historic global biomass burning emissions for CMIP6 (BB4CMIP) based on merging satellite observations with proxies and fire models (1750–2015), *Geosci. Model Dev.*, 10, 3329–3357, <https://doi.org/10.5194/gmd-10-3329-2017>, 2017.
- van der Werf, G. R., Randerson, J. T., Giglio, L., Collatz, G. J., Kasibhatla, P. S., and Arellano Jr., A. F.: Interannual variability in global biomass burning emissions from 1997 to 2004, *Atmos. Chem. Phys.*, 6, 3423–3441, <https://doi.org/10.5194/acp-6-3423-2006>, 2006.
- van der Werf, G. R., Randerson, J. T., Giglio, L., Gobron, N., and Dolman, A. J.: Climate controls on the variability of fires in the tropics and subtropics, *Global Biogeochem. Cy.*, 22, GB3028, <https://doi.org/10.1029/2007GB003122>, 2008.
- van der Werf, G. R., Randerson, J. T., Giglio, L., van Leeuwen, T. T., Chen, Y., Rogers, B. M., Mu, M., van Marle, M. J. E., Morton, D. C., Collatz, G. J., Yokelson, R. J., and Kasibhatla, P. S.: Global fire emissions estimates during 1997–2016, *Earth Syst. Sci. Data*, 9, 697–720, <https://doi.org/10.5194/essd-9-697-2017>, 2017.
- Wang, S. S.-C., Qian, Y., Leung, L. R., and Zhang, Y.: Interpreting machine learning prediction of fire emissions and comparison with FireMIP process-based models, *Atmos. Chem. Phys.*, 22, 3445–3468, <https://doi.org/10.5194/acp-22-3445-2022>, 2022.
- Wang, S. S.-C., Leung, L. R., and Qian, Y.: Projection of Future Fire Emissions Over the Contiguous US Using Explainable Artificial Intelligence and CMIP6, *J. Geophys. Res.*, 128, e2023JD039154, <https://doi.org/10.1029/2023JD039154>, 2023.
- Ward, D. S., Kloster, S., Mahowald, N. M., Rogers, B. M., Randerson, J. T., and Hess, P. G.: The changing radiative forcing of fires: global model estimates for past, present and future, *Atmos. Chem. Phys.*, 12, 10857–10886, <https://doi.org/10.5194/acp-12-10857-2012>, 2012.
- Ward, D. S., Shevliakova, E., Malyshev, S., and Rabin, S.: Trends and variability of global fire emissions due to historical anthropogenic activities, *Global Biogeochem. Cy.*, 32, 122–142, <https://doi.org/10.1002/2017GB005787>, 2018.
- Wiedinmyer, C., Kimura, Y., McDonald-Buller, E. C., Emmons, L. K., Buchholz, R. R., Tang, W., Seto, K., Joseph, M. B., Barsanti, K. C., Carlton, A. G., and Yokelson, R.: The Fire Inventory from NCAR version 2.5: an updated global fire emissions model for climate and chemistry applications, *Geosci. Model Dev.*, 16, 3873–3891, <https://doi.org/10.5194/gmd-16-3873-2023>, 2023.
- Williams, A. P., Abatzoglou, J. T., Gershunov, A., Guzman-Morales, J., Bishop, D. A., Balch, J. K., and Lettenmaier, D. P.: Observed Impacts of Anthropogenic Climate Change on Wildfire in California, *Earths Future*, 7, 892–910, <https://doi.org/10.1029/2019ef001210>, 2019.
- Wu, C., Sitch, S., Huntingford, C., Mercado Sergey Venevsky, L. M., Lasslop, G., Archibald, S., and Staver, A. C.: Reduced global fire activity due to human demography slows global warming by enhanced land carbon uptake, *P.Natl. Acad. Sci. USA*, 119, e2101186119, <https://doi.org/10.1073/pnas.2101186119>, 2022.
- Xie, Y., Lin, M., Decharme, B., Delire, C., Horowitz, L. W., Lawrence, D. M., Li, F., and Seferian, R.: Tripling of western US particulate pollution from wildfires in a warming climate, *P. Natl. Acad. Sci. USA*, 119, 2111372119, <https://doi.org/10.1073/pnas.2111372119>, 2022.
- Yu, Y., Mao, J., Wullschleger, S. D., Chen, A., Shi, X., Wang, Y., Hoffman, F. M., Zhang, Y., and Pierce, E.: Machine learning-based observation-constrained projections reveal elevated global socioeconomic risks from wildfire, *Nat. Commun.*, 13, 1250, <https://doi.org/10.1038/s41467-022-28853-0>, 2022.
- Yukimoto, S., Kawai, H., Koshiro, T., Oshima, N., Yoshida, K., Urakawa, S., Tsujino, H., Deushi, M., Tanaka, T., Hosaka, M., Yabu, S., Yoshimura, H., Shindo, E., Mizuta, R., Obata, A., Adachi, Y., and Ishii, M.: The Meteorological Research Institute Earth System Model version 2.0, MRI-ESM2.0: Description and basic evaluation of the physical component, *J. Meteor. Soc. Jpn.*, 97, 931–965, <https://doi.org/10.2151/jmsj.2019-051>, 2019.
- Zheng, B., Ciais, P., Chevallier, F., Chuvieco, E., Chen, Y., and Yang, H.: Increasing forest fire emissions despite the decline in global burned area, *Sci. Adv.*, 7, eabh2646, <https://doi.org/10.1126/sciadv.abh2646>, 2021.